Highly Selective PTK2 Proteolysis Targeting Chimeras to Probe Focal Adhesion Kinase Scaffolding Functions

Popow, Johannes; Arnhof, Heribert; Bader, Gerd; Berger, Helmut; Ciulli, Alessio; Covini, David

Published in:
Journal of Medicinal Chemistry

DOI:
10.1021/acs.jmedchem.8b01826

Publication date:
2019

Document Version
Peer reviewed version

Article

Highly Selective PTK2 Proteolysis Targeting Chimeras (PROTACs) to Probe Focal Adhesion Kinase Scaffolding Functions

Johannes Popow, Heribert Arnhof, Gerd Bader, Helmut Berger, Alessio Ciulli, David Covini, Christian Dank, Teresa Gmaschitz, Peter Greb, Jale Karolyi-Oezguer, Manfred Koegl, Darryl McConnell, Mark Pearson, Maria Rieger, Jörg Rinnenthal, Vanessa Roessler, Andreas Schrenk, Markus Spina, Steffen Steurer, Nicole Trainor, Elisabeth Traxler, Corinna Wieshofer, Andreas Zoephel, and Peter Ettmayer

J. Med. Chem., **Just Accepted Manuscript** • DOI: 10.1021/acs.jmedchem.8b01826 • Publication Date (Web): 09 Feb 2019

Highly Selective PTK2 Proteolysis Targeting Chimeras (PROTACs) to Probe Focal Adhesion Kinase Scaffolding Functions.

*Johannes Popow[1], Heribert Arnhof[1], Gerd Bader[1], Helmut Berger[1], Alessio Ciulli[2], David Covini[1], Christian Dank[1], Teresa Gmaschitz[1], Peter Greb[1], Jale Karolyi-Özguer[1], Manfred Koegl[1], Darryl B. McConnell[1], Mark Pearson[1], Maria Rieger, Joerg Rinnenthal[1], Vanessa Roessler[1], Andreas Schrenk[1], Markus Spina[1], Steffen Steurer[1], Nicole Trainor[2], Elisabeth Traxler[1], Corinna Wieshofer[1], Andreas Zoephel[1], Peter Ettmayer[1]**

[1] Boehringer Ingelheim RCV GmbH & Co KG, 1221 Vienna, Austria

[2] Division of Biological Chemistry and Drug Discovery, School of Life Sciences, James Black Centre, University of Dundee, Dow Street, DD1 5EH, Dundee, Scotland, United Kingdom

*corresponding author, E-mail: peter.ettmayer@boehringer-ingelheim.com

KEYWORDS

PROTACs, protein degradation, E3 ubiquitin ligases, kinases, von Hippel-Lindau, Cereblon, CRBN

ABSTRACT

The focal adhesion tyrosine kinase (PTK2) is often over-expressed in human hepatocellular carcinoma (HCC) and several reports have linked PTK2 depletion and/or pharmacological inhibition to reduced tumorigenicity. However, the clinical relevance of targeting PTK2 still remains to be proven. Here we present two highly selective and functional PTK2 PROTACs utilizing VHL and cereblon ligands to hijack E3 ligases for PTK2 degradation. BI-3663 (cereblon-based) degrades PTK2 with a median DC_{50} of 30 nM to > 80 % across a panel of eleven HCC cell lines. Despite effective PTK2 degradation, these compounds did not phenocopy the reported anti-proliferative effects of PTK2 depletion in any of the cell lines tested. By disclosing these compounds, we hope to provide valuable tools for the study of PTK2 degradation across different biological systems.

Introduction

Focal adhesion tyrosine kinase (PTK2) is a cytoplasmic protein tyrosine kinase that is overexpressed and activated in many types of advanced-stage solid cancers. PTK2 is reported to play an important role in adhesion, spreading, motility, invasion, metastasis, survival, angiogenesis, epithelial to mesenchymal transition (EMT), cancer stem cells and the tumour microenvironment[1,2]. Overexpression and activation of PTK2 is associated with several human malignant diseases, including colorectal[3], ovarian[4], esophageal[5] and hepatocellular carcinoma (HCC)[6] and is correlated with poor overall patient survival[7, 8]. Hepatocellular carcinoma (HCC) is the most common type of liver cancer in humans, accounting for 70–85 % of primary liver malignancies, and is the third leading cause of cancer-related death worldwide[9, 10]. HCC is associated with an extremely poor prognosis since it is often diagnosed at advanced stages, restricting the currently available therapeutic options to either surgical resection or liver transplantation[11, 12]. Several reports link PTK2 depletion or pharmacological inhibition of its kinase activity to reduction of *in vitro* and *in vivo* tumorigenicity in HCC models[13, 14]. However, the disconnect between modulation of intracellular PTK2 autophosphorylation and growth inhibition as well as the often suboptimal selectivity profile of the inhibitors used makes it difficult to link the reported blockade of HCC tumour initiation and maintenance to PTK2 inhibition.

We previously described BI-853520, a novel ATP-competitive inhibitor distinguished by high potency and selectivity[15, 16]. BI-853520 inhibits PTK2 autophosphorylation in cancer cell lines and blocks anchorage-independent proliferation with single digit nmol/L potency. In contrast, cells grown in conventional surface (2-D) culture were found to be 1,000-fold less sensitive to BI-853520. These findings are in keeping with the described role of PTK2 in integrin mediated

signaling[2, 17]. We reasoned that ligands derived from BI-853520 would be suitable to develop PROTACs (PROteolysis TArgeting Chimeras) and compare the potential anti-oncogenic effects of PTK2 depletion as compared to inhibition of its kinase activity[18].

PROTACs are bifunctional degrader molecules composed of a ligand for the target protein linked to a module that recruits an E3 ligase[19, 20]. PROTACs represent an emerging therapeutic strategy to use small molecules to deplete a protein by repurposing the ubiquitin-proteasome system[21, 22]. Upon formation of a ternary complex target:PROTAC:E3 ligase[23-25], the protein of interest is ubiquitinated and subsequently degraded by the proteasome. Compared to pharmacological inhibition of the kinase function, protein degradation more closely resembles genetic approaches to interfere with PTK2 expression in HCC models. Moreover, PROTAC molecules can add a layer of target selectivity beyond that expected from the constitutive binding ligands, thus providing highly selective degraders with potentially reduced off-target effects[25-28].

The most common E3 ligases currently recruited using PROTACs are the von Hippel-Lindau (VHL) protein complex $CRL2^{VHL}$ and the cereblon (CRBN) complex $CRL4^{CRBN}$. PROTACs consisting of the same target ligand but employing either VHL or CRBN ligands can exhibit different degradation selectivity and efficacy[26, 29-31]. Emerging evidence suggests that it might be beneficial to develop parallel chemical series hijacking different E3 ligases. First, expression of the recruited E3 ligase and intrinsic activity may be context-dependent and vary widely amongst cell- and tissue types[32]. Second, resistance mechanisms could potentially arise from loss of the recruited E3 ligase, as demonstrated by the correlation between level of CRBN and response to CRBN-recruiting drugs in multiple myeloma[33]. Flexible choice of the recruited E3 ligase may therefore aid targeted protein degradation.

Recently, the first PTK2 PROTACs have been reported. Conjugating the known pyrimidine-based ALK inhibitors, TAE684 and LDK378, to the cereblon ligand pomalidomide led to the discovery of the first small molecule degraders of ALK that concomitantly degrade, PTK2, Aurora A, FER, and RPS6KA1[34]. A PROTAC based on a highly promiscuous kinase inhibitor was also reported to degrade PTK2 amongst 27 additional kinases[35]. While both studies demonstrate that PTK2 can be targeted by a PROTAC approach, they also clearly highlight the need for more selective PTK2 PROTACs to address its role in cancer. Motivated by the potential of targeting kinase-independent functions of PTK2 with a low molecular weight modality, we initiated a PROTAC medicinal chemistry campaign to artificially recruit PTK2 to two different E3 ligases.

Here, we show the synthesis and characterization of the first probe-quality PROTACs targeting PTK2. Structure-guided conjugation of a highly selective PTK2 inhibitor to either a CRBN or VHL ligand led to selective PTK2 degraders. We profiled both PROTACs for degradation efficacy and anti-proliferative activity in a panel of HCC, tongue squamous cell carcinoma, melanoma, pancreatic ductal adenocarcinoma and non-small cell lung cancer cell lines several of which were recently shown to depend on expression of PTK2 by functional RNA interference screening[36]. Despite potent and complete degradation of PTK2, both degraders failed to show the anticipated growth reduction beyond the effect of a PTK2 kinase inhibitor in these models.

Results and Discussion

We designed a set of PTK2 PROTACs recruiting the two E3 ubiquitin ligases, VHL and CRBN, to test whether PTK2 can be targeted by targeted proteolysis. Making use of available E3 ligase ligands, we aimed at maximizing the chance of developing an active PTK2 degrader tool compound. We selected the highly selective ATP competitive inhibitor BI-4464 (**1**, Scheme 1), a

close analogue of the 2-aminophenyl-4-phenoxypyrimidine BI-853520[15] currently being tested in clinical trials as a PTK2 ligand. The choice of BI-4464 as a target ligand was driven by its high binding affinity and exquisite selectivity across a large kinase panel (see also Figure 3). We believe that this exceptional selectivity originates from a unique binding mode which seems to be less tolerated by other kinases. To design a first generation of degraders, we inspected the crystal structure of BI-4464 bound to the PTK2 kinase domain to identify suitable attachment points and vectors for linker conjugation (Figure 1). The structure shows binding of the trifluoro-aminopyrimidine moiety to the backbone nitrogen and carbonyl of cysteine 502 in the hinge region via two hydrogen bonds. In addition, the oxygen of the dihydroindenone moiety forms another hydrogen bond to the backbone nitrogen of aspartic acid 564. The N-methyl piperidine group of BI-4464 was identified as solvent-exposed and not involved in any interactions with the protein. We further selected **2**[37] and pomalidomide **3**,[38] (Scheme 1) as VHL and CRBN ligands, respectively. Their terminal amino groups (Table 1 and Scheme 1) were conjugated *via* an amide bond to the linker consisting of up to five PEG units without perturbing the interaction with the E3 ligases, as previously demonstrated[28, 31, 39, 40].

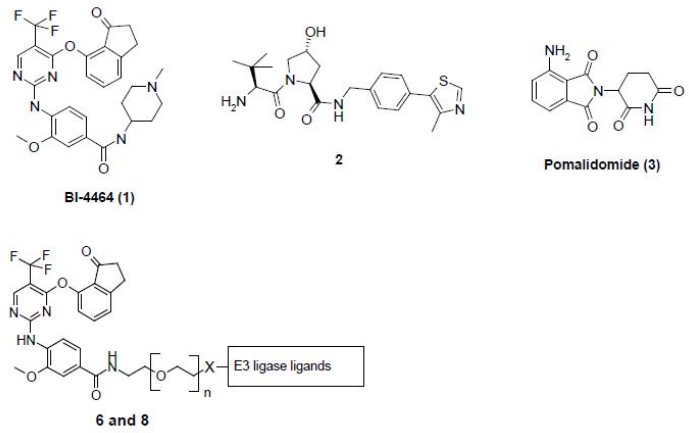

Scheme 1. Chemical structures of BI-4464 ligand **1**, VHL ligand **2**[37, 41, 42] and CRBN ligand **3**[38].

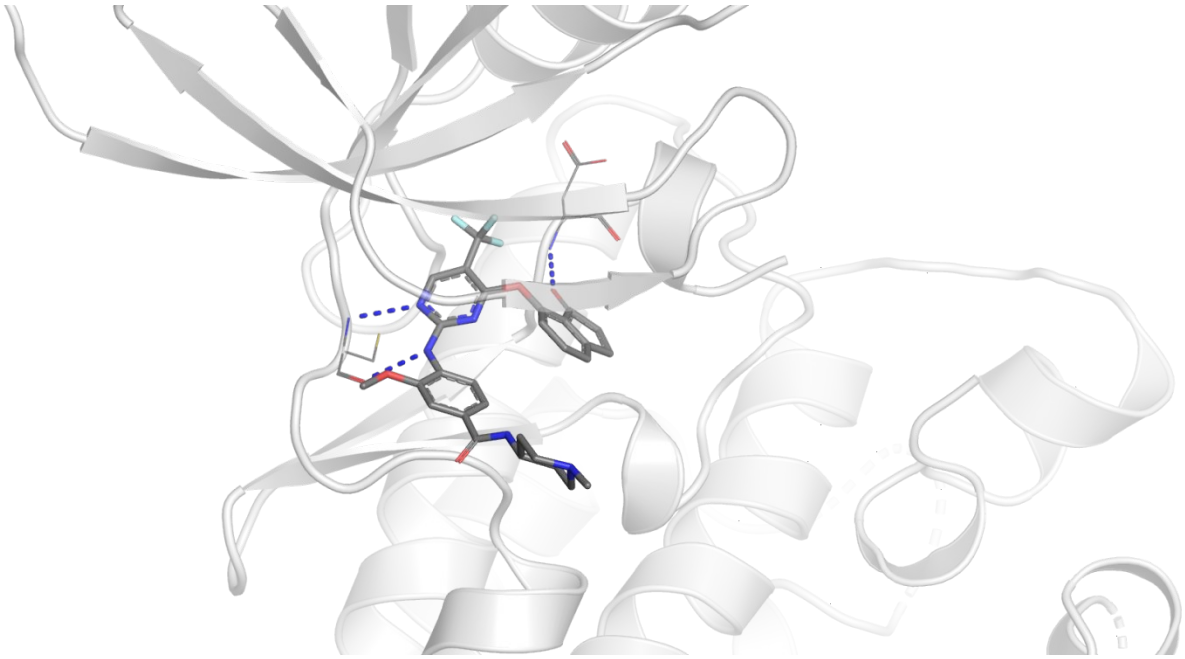

Figure 1. Structure of BI-4464 bound to PTK2 (PDB ID 6I8Z). Hydrogen bonds to cysteine 502 and aspartic acid 564 are depicted in blue.

To obtain the described compounds **6** and **8** (Table 1), a convergent synthesis was developed to connect **1a** to each E3 ligase ligand **2** and **3**. PEG linkers 1-5 (Scheme 2 shows an example of linker length three) were synthesized and profiled. The synthesis of ligand **1a** was carried out as outlined in Scheme 2. Aromatic nucleophilic substitution of the 4-chloropyrimidine **4** with 7-hydroxy-2,3-dihydroindan-1-one produced the carboxylic acid **1a.** Amide coupling of azido-PEG-3-propanoic acid and azido-PEG-3-acetic acid to the E3 ligase ligand **2** and **3** followed by catalytic hydrogenation produced the amines **5b**, **7b** and **10b** in good yields. The final PROTACs **6**, **8** and the cis-VHL analogue **11** were synthesized following amide coupling of the ligase linker conjugates **5**b, **7b** and **10b** with **1a.**

Table 1. Binary affinities of compounds **1**, **6**, **8** for PTK2 and the respective PTK2 degradation data in A549 cells.

Code	N	X	E3 ligase ligand	PTK2* pIC_{50}	A549 cells, 18h**	
					pDC_{50}	D_{max} [%]
1 (BI-4464)	-	-	-	7.8 ± 0.1	>10,000	-
6 (BI-3663)	3	CONH	POMA	7.7 ± 0.1	7.6 ± 0.1	95 ± 4
8 (BI-0319)	2	O-CH_2-CONH	2	7.7 ± 0.1	6.7 ± 0.4	80 ± 9

* Thermo Fisher selectScreen Kinase Profiling Services, Z´-Light, ATP@Km, pIC50 ± STDEV ** Degradation activity is reported as concentration needed to achieve 50 % PTK2 protein degradation (pDC_{50} ± STDEV) and maximal achievable protein degradation (D_{max}) relative to DMSO. PTK2 levels were determined by protein capillary electrophoresis and normalized to GAPDH. ($N = 3$)

Scheme 2. Synthesis of the PTK2 degraders.[a]

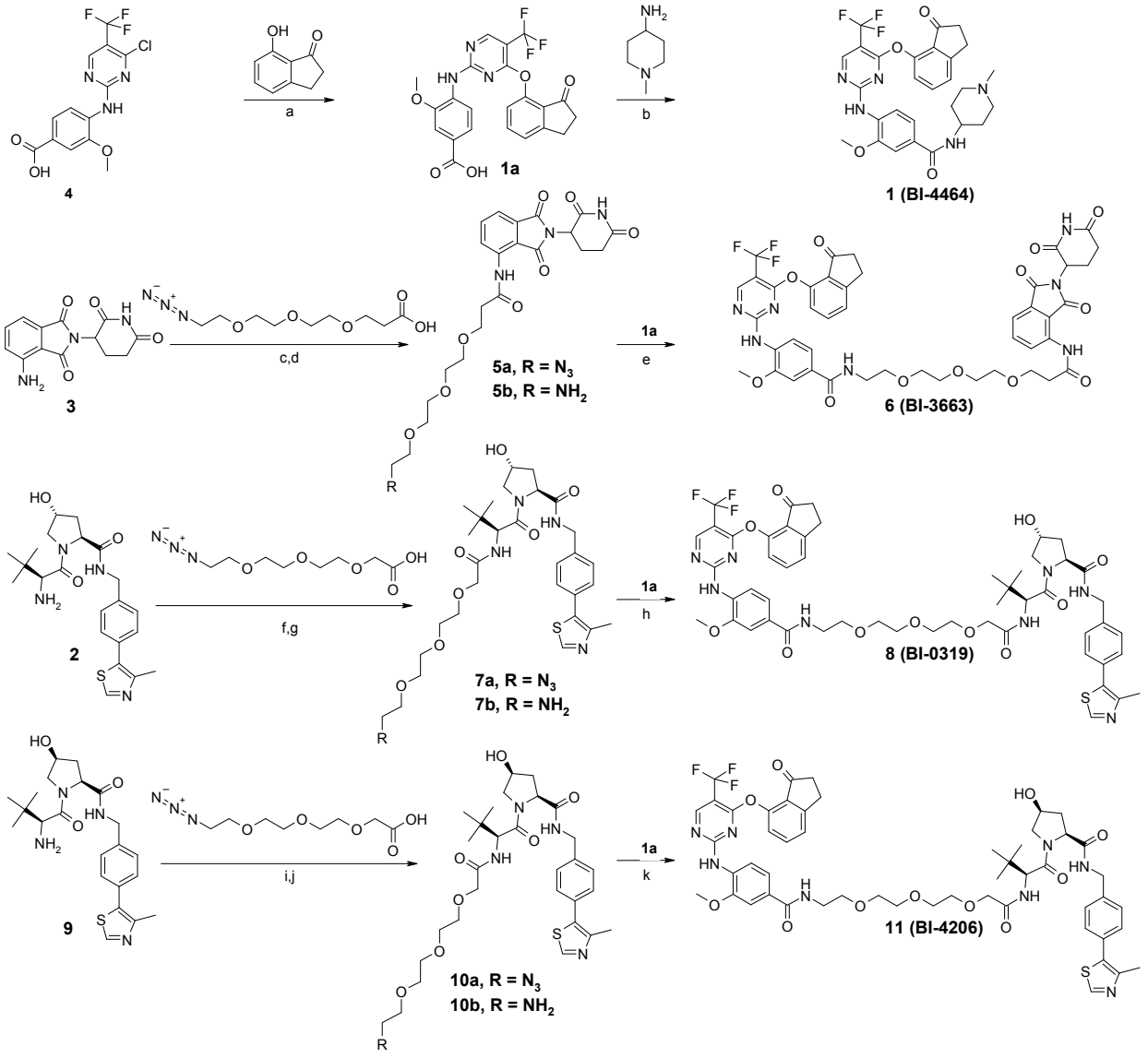

[a]Reaction Conditions: (a) Cs_2CO_3, $MgSO_4$, dioxane, 80°C, 16 h, 78%; (b) HATU, DIPEA, DMF, rt, 2 h, 75%; (c) T3P, pyridine, DMF, 80°C, 3h, 76%; (d) H_2 (6 bar), Pd/C (10%), MeOH, rt, 3 h, 90%; (e) **1a**, HATU, DIPEA, DMF, rt, 18 h, 10%; (f) HATU, DIPEA, DMF, rt, 1 h, 63%; (g) H_2 (5 bar), Pd/C (10%), MeOH, rt, 2.5 h, 82%; (h) **1a**, HATU, DIPEA, DMF, rt, 24 h, 34%; (i) HATU, DIPEA, DMF, rt, 2 h, 47%; (j) H_2 (6 bar), Pd/C (10%), MeOH, rt, 3 h, 98%; (k) **1a**, HATU, DIPEA, DMF, rt, 16 h, 69%.

We next tested PTK2 degradation by all synthesized PROTACs (sampling linker lengths of up to five ethylene glycol units) after 16 hours treatment of the human lung adenocarcinoma cell line A549. PROTACs **6** (BI-3663) and **8** (BI-0319) were identified as the best degraders in the CRBN and VHL series and characterized in greater detail. The CRBN-based PROTAC **6** (BI-3663) degraded PTK2 potently (DC_{50} = 27 nM) with a maximally obtainable degradation at the chosen experimental conditions of 95% (D_{max}) while the best VHL-based PROTAC **8** (BI-0319) only achieved partial degradation (D_{max} = 80 %) and was less potent (DC_{50} = 243 nM) in A549 cells (Table 1 and Figure 2). Further, both PROTACs show a small apparent hook effect in A549 cells at 25 μM. Consistent with VHL dependency, which requires the substituents of the pyrrolidine in the VHL ligand in a *trans* configuration[28], degradation of PTK2 by **8** (BI-0319) was abolished by switching the stereochemistry of the pyrrolidine substituents to the *cis* configuration (**11, BI-4206**) (Figure 2A). Moreover, as predicted for neddylation-dependent E3 ligases such as VHL and CRBN, the NEDD8 inhibitor MLN4924[43] (MLN) inhibited degradation of PTK2 by **6** (BI-3663) and **8** (BI-0319) (Figure 2A and B). Importantly, the PTK2 ligand **1** itself did not affect PTK2 levels**.**

We assessed PTK2 target engagement *in vitro* to understand the effect of the linker and exit vector on PTK2 inhibition of PROTACs **6** and **8**. As predicted from the structure-based design, both PROTACs and the PTK2 ligand inhibited PTK2 *in vitro* with virtually identical potencies (IC_{50} = 18 and 19 versus 17 nM for the PTK2 inhibitor **1**).

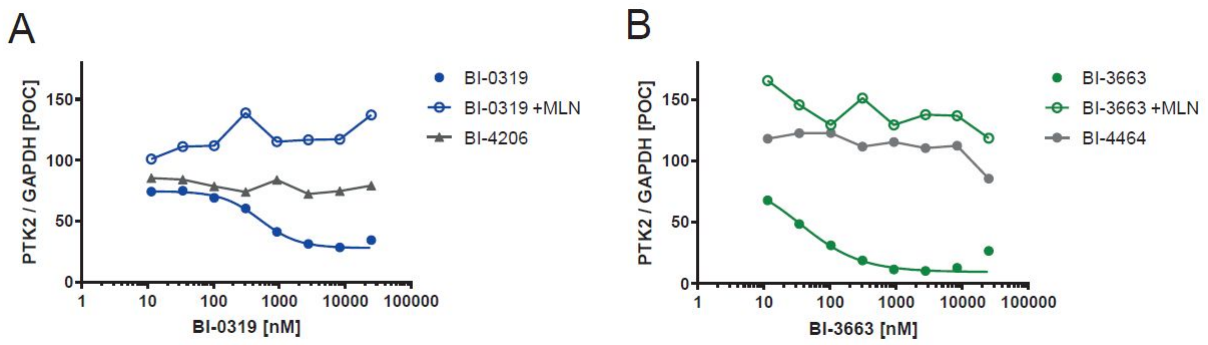

Figure 2. Characterization of BI-0319 and BI-3663 in A549 cells. A) A549 cells were treated with the indicated concentrations of BI-0319 in presence or absence of the NEDD8 inhibitor MLN4924 (MLN, 3 μM) or an inactive stereoisomer (BI-4206) for 18 h. PTK2 levels were determined by protein capillary electrophoresis and normalized to GAPDH. Values are stated as percentages of DMSO controls (POC). B) A549 cells were treated with the indicated concentrations of BI-3663 in presence or absence of the NEDD8 inhibitor MLN4924 (3 μM) or with the PTK2 inhibitor BI-4664 for 18 h. PTK2 levels were measured and are stated as in A.

In contrast to the previously published less selective PTK2 degraders[34, 35], we believe that a defining aspect of the PTK2 degraders described here is their high selectivity, which should enable validation of the relevance of PTK2 scaffolding functions in biologically relevant contexts. Indeed, of the 397 kinases tested in a kinase panel screening only 2 were inhibited by more than 90 % at 1 μM (Figure 3). Interestingly, BI-0319 (**8**) is more selective than the already highly selective PTK2 TKI **1** (BI-4464). We assume that the kinase selectivity panel for BI-3663 (**6**) might be comparable to BI-0319 since both exit vector and linker are identical for a distance of nine atoms from the piperidine moiety of the PTK2 ligand

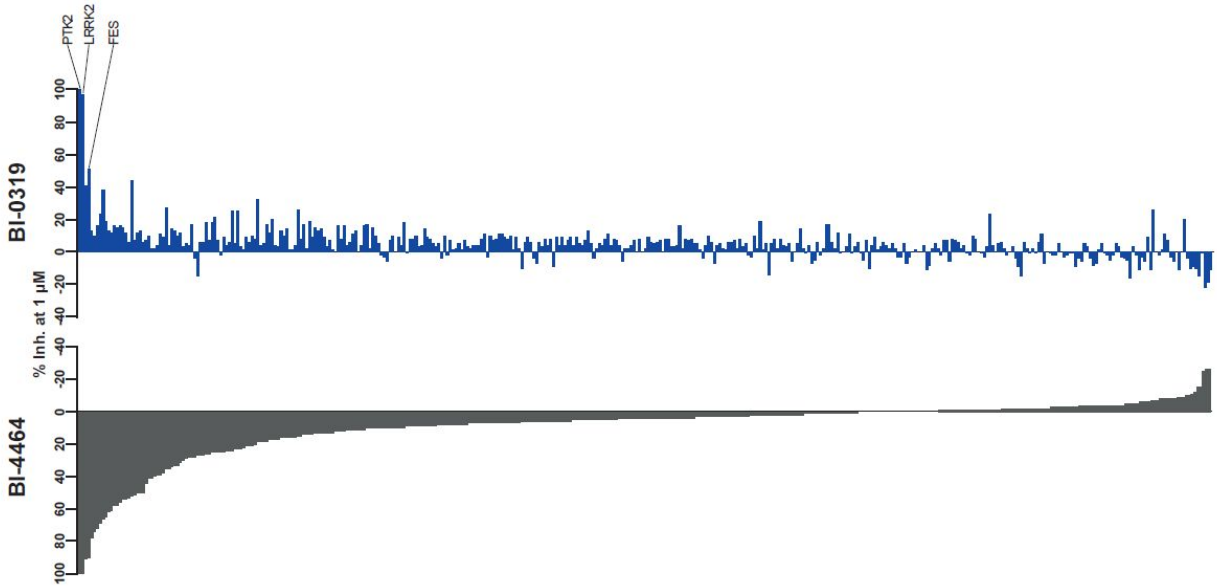

Figure 3. Kinase selectivity panels of the PTK2 ligand BI-4464 and VHL PROTAC BI-0319. Bars indicate percent inhibition at 1 µM of either compound.

We employed multiplexed isobaric tagging mass spectrometry to assess the cellular selectivity of BI-3663 (**6)** and BI-0319 (**8**) for PTK2 degradation and identify potential degradation off-targets in a quantitative and unbiased manner. Amongst the 6,008 proteins quantified in this analysis in A549 cells, PTK2 showed a distinct and significant change in abundance upon treatment with either PROTAC. (Figure 4 and Supplemental table 3). Neither BI-3663 (**6**) nor BI-0319 (**8**) induced any significant changes in abundance of other detectable kinases, thus confirming the high selectivity of both degraders within the kinase family. Of note, the two most prominent kinase off-targets of the inhibitor were not detected in this dataset. Interestingly BI-0319 (**8**) – but not BI-3663 (**6**) – also induced a significant change of PDE6D levels (Figure 4A), a finding corroborated by immunoblot in A549 cells (Supplemental figure 1).

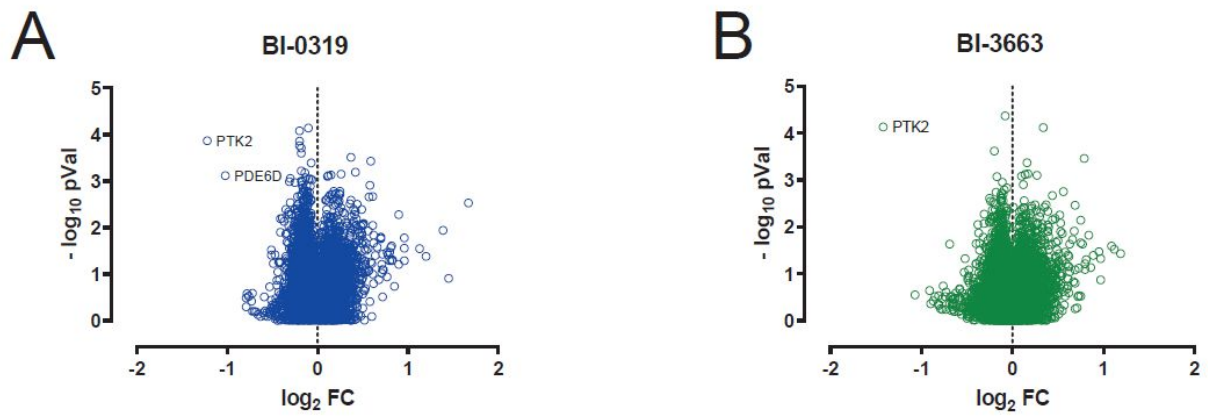

Figure 4. Total proteome analysis of A549 cells treated with 3 µM of BI-0319 (A) or BI-3663 (B) for 18 h and compared to DMSO controls. Samples were run in biological triplicates and analyzed by mass spectrometry. Volcano plot displays log2 of fold-change in abundance versus – log10 of adjusted p value ($N = 3$).

Having established the high selectivity of both PROTACs, in particular of the CRBN-based BI-3663**,** we tested their potential to degrade PTK2 in a panel of eleven HCC cell lines (Table 3 and Supplemental figure 2 and 3). Both PROTACs show comparable degradation potencies and efficacies in the 11 HCC cell lines tested (BI-3663 mean pDC50 = 7.45±0.60 versus BI-0319 mean pDC50 = 7.08±0.52). Whereas PTK2 levels in cell lines such as SNU-398 were equally sensitive to treatment with both PROTACs, other cell lines, such as Hep3B2.1-7 exhibited a >10 fold difference of the potencies of **6** and **8** in cell-based PTK2 degradation assays, as observed for A549 cells during the profiling experiments (Figure 5 and Table 2).

It is not unexpected that heterobifunctional molecules unavoidably result in high molecular weight compounds, making it difficult to balance their physicochemical properties in a manner

consistent with acceptable permeability and solubility. While both PROTACs have a comparable low aqueous solubility and high tPSA (241,243 Å2), PROTAC **6** has one hydrogen bond donor (HBD) more than PROTAC **8.** The negative impact on permeability for **6** might be compensated by the higher lipophilicity (ClogP 6.9 vs 3.8) however, the higher lipophilicity of **6** also translates in higher PPB and lower free fraction (**6**: 4.0%, **8**: 11.3; Supplemental table 1).

As assessed by the Caco2 assay, both PROTACs exhibit low permeability and significant efflux (Supplemental table 1). Therefore, high efflux might compromise cellular exposures achieved by both PROTACs. We reasoned that blocking multidrug efflux pumps (such as the Multidrug-Resistance-Protein 1, PGP) might boost the potency and efficacy of both PROTACs in cell lines with a large discrepancy between biochemical and intracellular activity. Cyclosporine A (CsnA) has been described as a substrate of several drug transporters including PGP[44] and can therefore be used to saturate these transporters at high concentrations. Consequently, we assessed PTK2 degradation by both PROTACs upon addition of CsnA to saturate drug transport in Hep3B2.1-7 (Figure 6A and B). Indeed, we observed a comparable shift in the potency of PTK2 degradation for both PROTACs (Table 2), consistent with efflux contributing to their reduced degradation efficacy in this cell line. Of note, CsnA only had a minor effect on PTK2 levels (Figure 6C).

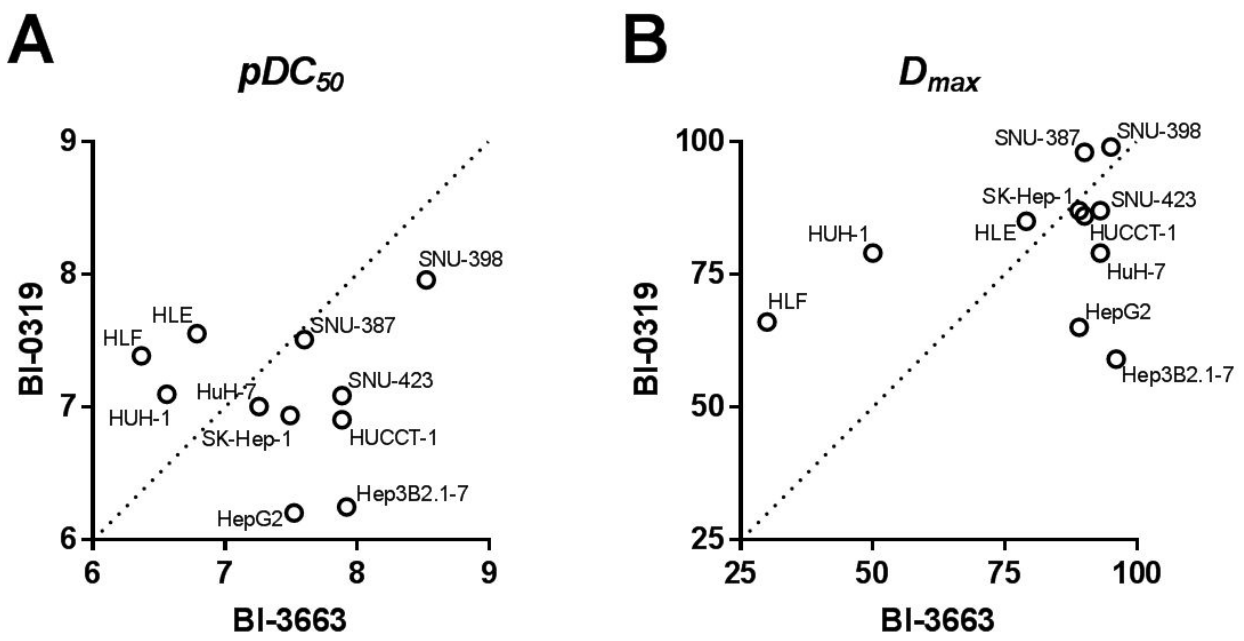

Figure 5. Cumulative analysis of half-maximal effective concentrations (DC_{50}, A) and maximal degree of PTK2 degradation (Dmax, B) achieved by BI-0319 or BI-3663. pDC_{50} and Dmax at 18 h were determined as indicated in supplemental figures 2 and 3.

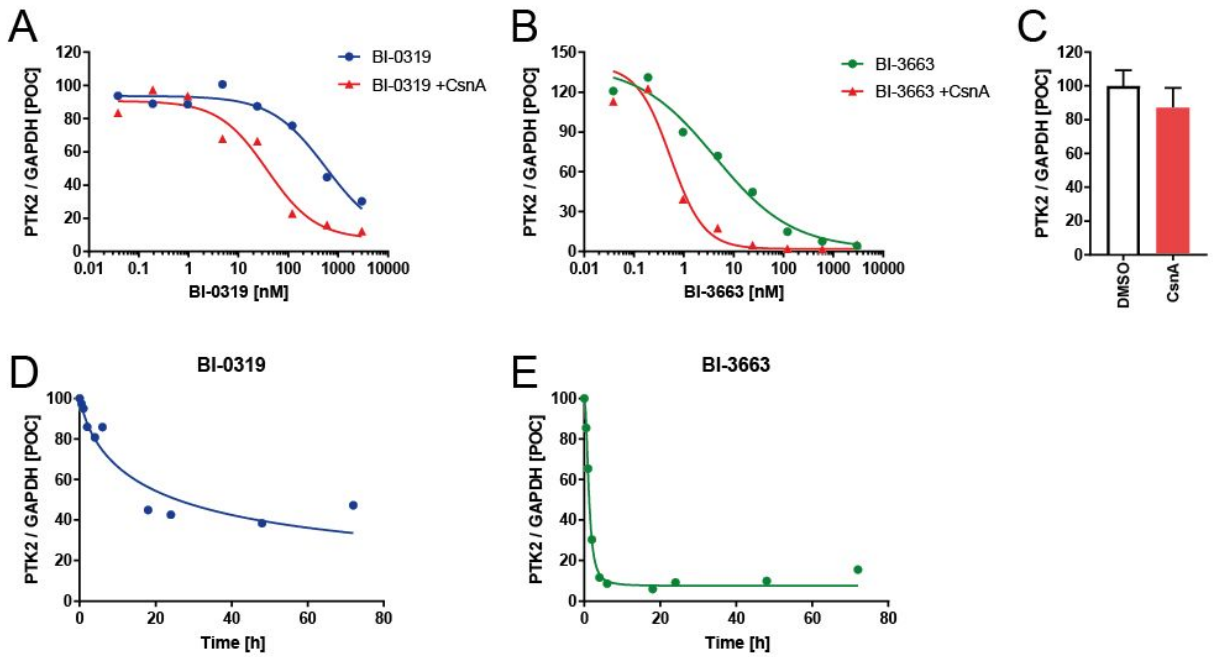

Figure 6. Analysis of PTK2 degradation in Hep3B2.1-7 cells. A) cells were treated with the indicated concentrations of BI-0319 for 18 h in presence (red triangles) or absence (blue circles) of 10 µM cyclosporine A (CsnA). B) cells were treated for 18 h with the indicated concentrations of BI-3663 in presence (red triangles) or absence (green circles) of 10 µM CsnA. C) cells were treated with 10 µM CsnA for 18 h. D) Time course analysis of PTK2 levels in cells treated with 3 µM BI-0319. E) Time course analysis of PTK2 levels in cells treated with 3 µM BI-3663. Values state PTK2 protein levels normalized to GAPDH relative to DMSO (or CsnA only) controls.

Table 2. PTK2 degradation data of BI-3663 and BI-0319 in A549 and Hep3B2.1-7 cells.

	A549, 18 h*		**Hep3B2.1-7, 18 h ***		**Hep3B2.1-7, 18 h * + 10 µM CsnA**	
	pDC_{50}	**D_{max} [%]**	**pDC_{50}**	**D_{max} [%]**	**pDC_{50}**	**D_{max} [%]**
6 (BI- 3663)	7.6 ± 0.1	95 ± 4	7.9	96	9.0	94
8 (BI -0319)	6.7 ± 0.4	80 ± 9	6.2	59	7.4	88

* Degradation activity is reported as concentration needed to achieve 50 % PTK2 protein degradation (pDC_{50} ± STDEV) and maximal achievable protein degradation (D_{max}) relative to DMSO.

PROTACs **6** and **8** differ considerably with respect to their cellular degradation rate in Hep3B2.1-7 cells. The CRBN-based PROTAC **6** achieved complete degradation of PTK2 after five hours whereas the VHL-based PROTAC **8** achieved maximal degradation only after 20 hours (Figure 6D and E). Of note, the CRBN-based PROTAC **6** was considerably less stable in cell assay buffer containing 10% FCS (M+18 and +32 observed) than the VHL-based PROTAC **8** (Supplemental Table 1). PROTAC 6 was found to be stable as a solid and in DMSO stock solution (>3 month, data not shown). Despite this previously reported instability of CRBN based PROTACs[45] PROATC **6** as well as PROTAC **8** showed comparable maximal degradation of PTK2 after 18 h and 72h days incubation (Supplemental figure 6). Taken together, this indicates that the both PROTACs **6** and **8** are suitable probes to further study the role of PTK2 in a broad range of tumour cell lines.

Reasoning that additional targeting of the scaffolding functions of PTK2 by PROTAC-mediated degradation might result in enhanced efficacy as compared to inhibition of its kinase activity, we next tested the effect of PROTAC-mediated PTK2 degradation on proliferation of the same HCC cell lines. Surprisingly, efficient depletion of PTK2 by both PROTACs (Table 3 and Supplemental figures 2 and 3) did not affect proliferation of the tested cell lines more severely than the PTK2 inhibitor BI-4464 in standard culture conditions or in anchorage-independent growth assays (Table 3, Supplemental figures 4 and 5). Notably, sensitivity to genetic depletion of PTK2 has been described for several of the tested cell lines (Supplemental table 4). One explanation may be that effects on proliferation may require long-term depletion of PTK2. To further address this, we treated cell lines with reported high sensitivity to genetic depletion of PTK2[36, 46] (Supplemental table 4) for 21 days with either PROTAC **6** (BI-3663) or **8** (BI-0319) or the PTK2 inhibitor **1** (BI-4464). Despite the effective depletion of PTK2 even after 21 days, we did not observe any pronounced anti-proliferative effects for any of the tested cell lines (Supplemental figure 6). Notably, CRISPR-based genetic validation in cultured HuH-1 cells also resulted in a weak dependency on PTK2 (Supplemental figure 7). Taken together, these data questions the scaffolding function of PTK2 being required for *in vitro* proliferation of the tested cell lines beyond the effect of inhibition of its kinase activity. Nevertheless, our observations indicate that both probes can be used to effectively reduce PTK2 protein levels in long term experiments in cultured cells.

Table 3. Degradation characteristics and effect on proliferation of BI-3663 (**6**) and BI-0319 (**8**) in HCC lines.

Cell line	BI-3663			BI-0319			BI-4464
	pDC_{50}	D_{max}, [%]	pIC_{50} (proliferation)	pDC_{50}	D_{max}, [%]	pIC_{50} (proliferation)	pIC_{50} (proliferation)
SNU-387	7.6	90.0	<4.6	7.5	98.0	5.3	5.2
HUH-1	6.6	50.0	4.6	7.1	79.0	4.7	5.4
Hep3B2.1-7	7.9	96.0	4.6	6.2	59.0	5.2	5.3
HepG2	7.5	89.0	<4.6	6.2	65.0	<4.6	5.5
SK-Hep-1	7.5	89.0	5.8	6.9	87.0	5.1	5.2
HLF	6.4	30.0	<4.6	7.4	66.0	<4.6	5.4
SNU-398	8.5	95.0	<4.6	8.0	99.0	5.1	5.2
HUCCT1	7.9	90.0	<4.6	6.9	86.0	5.2	5.2
HLE	6.8	79.0	<4.6	7.6	85.0	5.0	5.1
HuH-7	7.3	93.0	<4.6	7.0	79.0	5.4	5.4
SNU-423	7.9	93.0	4.7	7.1	87.0	5.2	5.4

Conclusion

We describe the development of two highly selective and functional PROTACs to degrade the PTK2 protein, a kinase of significant relevance to cancer research, in particular, in the area of hepatocellular carcinoma. Structure-guided conjugation of a highly selective PTK2 inhibitor BI-4464 to either a CRBN or VHL ligand via polyethylene glycol linkers led to the selective PTK2 degraders BI-0319 and BI-3663, respectively, using orthogonal E3 ligase binders. Both PROTACs were characterized with respect to *in vitro* PTK2 engagement, ligase dependence

selectivity (kinase inhibition as well as whole cell proteome) and degradation efficacy (DC_{50} and D_{max}) in twelve cell lines (one lung cancer and eleven hepatocellular carcinoma cell lines). Both PROTACs are highly selective E3 ligase-dependent PTK2 degraders and show overall comparable potencies and efficacies of PTK2 degradation in the 12 cell tested lines. Whereas PTK2 levels in cell lines such as SNU-398 were equally sensitive to treatment with both PROTACs, other cell lines, such as Hep3B2.1-7 exhibited a more than ten-fold difference in cellular potency**.** This difference in degradation efficacy in Hep3B2.1-7 cells was associated with a higher degradation rate of BI-3663. Despite the efficient depletion of PTK2, treatment with either PROTAC did not affect proliferation of the tested cell lines in either short or long term assays in vitro (6 vs 21 days) beyond the effect achieved by a PTK2 kinase inhibitor. Taken together, these data suggest that PROTACs **6** (BI-3663) and **8** (BI-0319) mediated PTK2 depletion is likely insufficient to affect proliferation in vitro under the conditions tested beyond the effect of inhibition of its kinase activity. Nevertheless, both probes provide valuable tools to effectively reduce PTK2 protein levels in experimental conditions that might be better suited to reveal and differentiate between kinase- dependent and -independent functions of PTK2. BI-3663, BI-0319 and its inactive control BI-4206 will be made available to all scientists via our open innovation portal opnMe.

EXPERIMENTAL SECTION

Chemistry. Synthesis. Unless otherwise indicated, all reactions were carried out in standard commercially available glassware using standard synthetic chemistry methods. Air-sensitive and moisture-sensitive reactions were performed under an atmosphere of dry nitrogen or argon with dried glassware. Commercial starting materials were used without further purification. Solvents used for reactions were of commercial "dry"- or "extra-dry" or "analytical" grade. All other solvents used were reagent grade.

The thin layer chromatography is carried out on ready-made silica gel 60 TLC plates on glass (with fluorescence indicator F-254) made by Merck. The preparative high pressure chromatography (RP-HPLC) is carried out on Gilson systems with columns made by Waters (names: Sunfire™ Prep C18, OBD™ 10 µm, 50x150 mm or XBridge™ Prep C18, OBD™ 10 µm, 50x150 mm) and YMC (names: Actus-Triart Prep C18, 5 µm, 30x50 mm). Different gradients of MeCN/H_2O are used to elute the compounds, for acidic conditions 0.1 % HCOOH is added to the water. For the chromatography under basic conditions the water is made alkaline as follows: 5 mL NH_4HCO_3 solution (158 g in 1 L H_2O) and 2 mL NH_3 (28 % in H_2O) are replenished to 1 L with H_2O.

All compounds had a purity >95% acording to HPLC and NMR analysis acquired with the systems and parameters stated in the following. HPLC samples were analyzed on an Agilent 1200 series LC system coupled with an Agilent 6140 mass spectrometer. Purity was determined via UV detection with a bandwidth of 170nm in the range from 230-400nm. LC parameters were as follows: Waters Xbridge C18 column, 2.5µm particle size, 2.1 x 20mm. Total run time 3.1 minutes, flow 1ml/min, column temperature 60°C and 5µl injections. Solvent A (20mM

NH_4HCO_3/ NH_3 pH 9), solvent B (MS grade acetonitrile). Start 10% B, gradient 10% - 95% B from 0.0 - 1.5min, 95% B from 1.5 - 2.0min, gradient 95% - 10% B from 2.0 – 2.1min.

NMR experiments were recorded on a Bruker Avance HD 500 MHz spectrometer equipped with a TCI cryoprobe at 298 K. Samples were dissolved in 600 µL DMSO-d_6 and TMS was added as an internal standard. 1D ^{1}H spectra were acquired with 30° excitation pulses and an interpulse delay of 4.2 sec with 64k data points and 20 ppm sweep width. 1D ^{13}C spectra were acquired with broadband composite pulse decoupling (WALTZ16) and an interpulse delay of 3.3 sec with 64 k data points and a sweep width of 240 ppm. Processing and analysis of 1D spectra was performed with Bruker Topspin 3.2 software. No zero filling was performed and spectra were manually integrated after automatic baseline correction. Chemical shifts are reported in ppm on the δ scale.

HSQC spectra were recorded on all samples to aid the interpretation of the data and to identify signals hidden underneath solvent peaks. Spectra were acquired with sweep widths obtained by automatic sweep width detection from 1D reference spectra in the direct dimension with 1k datapoints and with 210 ppm, and 256 datapoints in the indirect dimension.

For HRMS a LTQ Orbitrap XL (Thermo Scientific) coupled with a Triversa Nanomate Nanospray ion source (ADVION Bioscience Inc.) was used.

3-methoxy-4-({4-[(3-oxo-2,3-dihydro-1H-inden-4-yl)oxy]-5-(trifluoromethyl)pyrimidin-2-yl}amino)benzoic acid (1a). 4-{[4-chloro-5-(trifluoromethyl)pyrimidin-2-yl]amino}-3-methoxybenzoic acid (**4**[47], 1.00g, 1eq) and 7-hydroxy-2,3-dihydro-1H-inden-1-one (879 mg, 2 eq) were taken up in dioxane (10 mL), then Cs_2CO_3 (4.686 g, 5 eq) was added. The reaction mixture was stirred at 80°C for 16 h. The reaction mixture was diluted with H_2O and acetonitrile

and concentrated under reduced pressure. The residue was purified by preparative RP-HPLC under basic conditions using MeCN/H2O as eluents in a gradient from 20:80 to 65:35 over 12 min. (column: XBridge™ Prep C18, OBD™ 10 µm, 50x150 mm; flow: 110 mL/min). Product containing fractions were freeze dried to give 3-methoxy-4-({4-[(3-oxo-2,3-dihydro-1*H*-inden-4-yl)oxy]-5-(trifluoromethyl)pyrimidin-2-yl}amino)benzoic acid (**1a**, 1.03 g, 78% yield) as brown solid. ^{1}H NMR (500 MHz, DMSO-d_6) δ = 12.85 (br s, 1H), 8.86 (s, 1H), 8.74 (s, 1H), 7.80 (t, *J*=7.88 Hz, 1H), 7.60 (d, *J*=7.88 Hz, 1H), 7.41 (d, *J*=0.95 Hz, 1H), 7.32 (br d, *J*=1.00 Hz, 1H), 7.24 (d, *J*=7.88 Hz, 1H), 7.15 (br d, *J*=1.00 Hz, 1H), 3.80 (s, 3H), 3.05-3.17 (m, 2H), two protons under DMSO. ^{13}C NMR (125 MHz, DMSO-d_6) δ = 203.4, 167.3, 166.4, 161.0, 158.4, 157.8, 149.7, 148.0, 137.0, 131.7, 128.9, 126.5, 125.5, 121.8, 121.1, 123.9, 120.4, 111.7, 101.5, 56.3, 36.7, 25.8. HRMS (*m/z*): $[M+H]^+$ calculated for $C_{22}H_{16}F_3N_3O_5$, 459.10421; found, 459.10411. HPLC-MS ^{t}R = 1.00 min.

3-methoxy-N-(1-methylpiperidin-4-yl)-4-({4-[(3-oxo-2,3-dihydro-1H-inden-4-yl)oxy]-5-(trifluoromethyl)pyrimidin-2-yl}amino)benzamide (1, BI-4464). In a glass vial, 3-methoxy-4-({4-[(3-oxo-2,3-dihydro-1*H*-inden-4-yl)oxy]-5-(trifluoromethyl)pyrimidin-2-yl}amino)benzoic acid (**1a**, 100 mg, 1 eq) was dissolved in DMF (1 mL). DIPEA (86 µl, 3 eq) and HATU (114 mg, 1.5 eq) were added. After the reaction mixture was stirred at rt for 5 min, 1-methylpiperidin-4-amine (46 mg, 52 µl, 2 eq) was added. The mixture was stirred at rt for 2 h. The reaction mixture was diluted with MeCN and H_2O and filtered through a syringe filter prior to purification *via* RP-HPLC under basic conditions using MeCN/H2O as eluents in a gradient from 30:70 to 98:2 over 8 min (column: YMC Actus-Triart Prep C18, 5 µm, 30x50 mm; flow: 50 mL/min). Product containing fractions were freeze dried to give 3-methoxy-*N*-(1-methylpiperidin-4-yl)-4-({4-[(3-oxo-2,3-dihydro-1*H*-inden-4-yl)oxy]-5-(trifluoromethyl)pyrimidin-2-yl}amino)benzamide (**1**,

(**BI-4464)**, 83 mg, 75% yield) as off-white lyophilizate. ^{1}H NMR (500 MHz, DMSO-d_6) δ = 8.83 (br s, 1H), 8.69 (s, 1H), 8.13 (d, *J*=7.57 Hz, 1H), 7.77 (dd, *J*=7.57, 7.88 Hz, 1H), 7.55 (d, *J*=7.57 Hz, 1H), 7.38 (d, *J*=0.95 Hz, 1H), 7.22 (d, *J*=7.88 Hz, 1H), 7.27 (br s, 1H), 7.12 (br s, 1H), 3.78 (s, 3H), 3.66-3.75 (m, 1H), 3.04-3.15 (m, 2H), 2.78 (br d, *J*=11.35 Hz, 2H), 2.16 (s, 3H), 1.85-1.98 (m, 2H), 1.69-1.80 (m, 2H), 1.49-1.65 (m, 2H), two protons under DMSO. ^{13}C NMR (125 MHz, DMSO-d_6) δ = 201.3, 164.2, 163.2, 159.1, 156.2, 155.7, 148.0, 145.8, 134.8, 128.8, 127.8, 126.8, 123.3, 118.8, 121.9, 117.5, 108.1, 99.0, 54.2, 53.0, 45.0, 44.4, 34.6, 29.9, 23.7, one carbon not detected. HRMS (*m/z*): $[M+H]^+$ calculated for $C_{28}H_{28}F_3N_5O_4$, 555.20934; found, 555.20824. HPLC-MS ^{t}R = 1.39 min.

3-{2-[2-(2-azidoethoxy)ethoxy]ethoxy}-N-[2-(2,6-dioxopiperidin-3-yl)-1,3-dioxo-2,3-dihydro-1H-isoindol-4-yl]propanamide (5a). In a 50 mL round-bottom flask, 4-amino-2-(2,6-dioxo-3-piperidyl)isoindoline-1,3-dione (500 mg, 1 eq) was dissolved in DMF (5 mL) and cooled to 0°C in an ice bath. 3-{2-[2-(2-azidoethoxy)ethoxy]ethoxy}propanoic acid (905 mg, 2 eq) was added dropwise. Then *N*-propylphosphonic acid anhydride, cyclic trimer (7.0 g, 6.5 mL, 6 eq) and pyridine (1.5 mL, 10 eq) were added. The mixture was stirred at 80°C for 3h. The reaction mixture was diluted with ACN/H_2O. The solution was filtered through a syringe filter and purified by preparative RP-HPLC under basic conditions using MeCN/H_2O as eluents in a gradient from 10:90 to 60:40 over 9 min. (column: XBridge™ Prep C18, OBD™ 10 µm, 50x150 mm; flow: 150 mL/min). Product containing fractions were freeze dried to give 3-{2-[2-(2-azidoethoxy)ethoxy]ethoxy}-*N*-[2-(2,6-dioxopiperidin-3-yl)-1,3-dioxo-2,3-dihydro-1*H*-isoindol-4-yl]propanamide (**5a**, 697 mg, 76% yield) as yellow lyophylizate. ^{1}H NMR (500 MHz, DMSO-d_6) δ = 11.15 (s, 1H), 9.88 (s, 1H), 8.54 (d, *J*=8.31 Hz, 1H), 7.83 (dd, *J*=7.26, 8.31 Hz, 1H), 7.62 (d, *J*=7.26 Hz, 1H), 5.14 (dd, *J*=5.52, 12.77 Hz, 1H), 3.74 (t, *J*=5.83 Hz, 2H), 3.52-3.61 (m, 6H),

3.47-3.52 (m, 4H), 3.34-3.37 (m, 2H), 2.84-2.96 (m, 1H), 2.70 (t, *J*=5.99 Hz, 2H), 2.53-2.66 (m, 2H), 2.00-2.12 (m, 1H). ^{13}C NMR (125 MHz, DMSO-d_6) δ = 173.2, 170.9, 170.2, 168.1, 167.1, 136.9, 136.6, 131.9, 126.5, 118.7, 117.1, 70.2, 70.2, 70.1, 70.1, 69.7, 66.6, 50.4, 49.4, 38.0, 31.4, 22.4. HRMS (*m/z*): $[M+H]^+$ calculated for $C_{22}H_{26}N_6O_8$, 502.18121; found, 502.18114. HPLC-MS ^tR = 1.05 min.

3-{2-[2-(2-aminoethoxy)ethoxy]ethoxy}-N-[2-(2,6-dioxopiperidin-3-yl)-1,3-dioxo-2,3-dihydro-1H-isoindol-4-yl]propanamide (5b). In a Parr-reactor 3-{2-[2-(2-azidoethoxy)ethoxy]ethoxy}-*N*-[2-(2,6-dioxopiperidin-3-yl)-1,3-dioxo-2,3-dihydro-1H-isoindol-4-yl]propanamide (**5a**, 190 mg, 1 eq) was dissolved in methanol (5 mL) and Pd/C (10%, 40 mg, 0.1 eq) was added. The reactor was flushed with N_2 and filled with H_2 (6 bar). The reaction mixture was stirred at rt for 3 h. A spoon of celite was added to the reaction mixture, the catalyst was filtered off through a celite pad and rinsed with DCM and MeOH. The filtrate was concentrated under reduced pressure. 3-{2-[2-(2-aminoethoxy)ethoxy]ethoxy}-*N*-[2-(2,6-dioxopiperidin-3-yl)-1,3-dioxo-2,3-dihydro-1*H*-isoindol-4-yl]propanamide (**5b**, 162 mg, 90% yield) was obtained as yellow resin. The product was taken to the next step without further purification. ^{1}H NMR (500 MHz, DMSO-d_6) δ = ppm 9.89 (br s, 1 H), 8.54 (d, *J*=8.20 Hz, 1 H), 8.36 (s, 1 H), 7.84 (dd, *J*=8.20, 7.25 Hz, 1 H), 7.62 (br d, *J*=7.25 Hz, 1 H), 5.14 (dd, *J*=12.93, 5.36 Hz, 1 H), 3.71 - 3.77 (m, 2 H), 3.45 - 3.60 (m, overlapped), 2.85 - 2.96 (m, 2 H), 2.82 (br t, *J*=5.36 Hz, 2 H), 2.71 (br t, *J*=5.83 Hz, 2 H), 2.02 - 2.11 (m, 1 H). ^{13}C NMR (125 MHz, DMSO-d_6) δ = 173.3, 170.9, 170.3, 168.1, 167.1, 136.9, 136.7, 131.9, 126.5, 118.8, 117.2, 70.2, 70.1, 70.1, 70.0, 69.2, 66.6, 49.4, 39.8, 38.0, 31.4, 22.4. HRMS (*m/z*): $[M+H]^+$ calculated for $C_{22}H_{28}N_4O_8$, 476.19071; found, 476.19041. HPLC-MS ^tR = 0.81 min.

N-[2-(2,6-dioxopiperidin-3-yl)-1,3-dioxo-2,3-dihydro-1H-isoindol-4-yl]-3-{2-[2-(2-{[3-methoxy-4-({4-[(3-oxo-2,3-dihydro-1H-inden-4-yl)oxy]-5-(trifluoromethyl)pyrimidin-2-yl}amino)phenyl]formamido}ethoxy)ethoxy]ethoxy}propanamide (6, BI-3663). In a glass vial, 3-methoxy-4-({4-[(3-oxo-2,3-dihydro-1*H*-inden-4-yl)oxy]-5-(trifluoromethyl)pyrimidin-2-yl}amino)benzoic acid (**2**, 170 mg, 1 eq) was dissolved in DMF (2 mL). DIPEA (150 µL, 3 eq) and HATU (155 mg, 1.2 eq) were added. The reaction mixture was stirred at rt for 5 min, then 3-{2-[2-(2-aminoethoxy)ethoxy]ethoxy}-*N*-[2-(2,6-dioxopiperidin-3-yl)-1,3-dioxo-2,3-dihydro-1*H*-isoindol-4-yl]propanamide (**5b**, 162 mg, 1eq) was added. The mixture was stirred at rt overnight. The reaction mixture was diluted with MeCN and H_2O and filtered through a syringe filter prior to purification *via* RP-HPLC under acidic conditions using MeCN/H2O as eluents in a gradient from 30:70 to 98:2 over 8 min (column: YMC Actus-Triart Prep C18, 5 µm, 30x50 mm; flow: 50 mL/min). Product containing fractions were freeze dried to give *N*-[2-(2,6-dioxopiperidin-3-yl)-1,3-dioxo-2,3-dihydro-1*H*-isoindol-4-yl]-3-{2-[2-(2-{[3-methoxy-4-({4-[(3-oxo-2,3-dihydro-1*H*-inden-4-yl)oxy]-5-(trifluoromethyl)pyrimidin-2-yl}amino)phenyl]formamido}ethoxy)ethoxy]ethoxy}propanamide (**6** (**BI-3663)**, 32 mg, 10% yield) as off-white lyophilizate. ^{1}H NMR (500 MHz, DMSO-d_6) δ = 11.13 (br s, 1H), 9.86 (s, 1H), 8.79 (br s, 1H), 8.70 (s, 1H), 8.53 (d, *J*=8.51 Hz, 1H), 8.43 (t, *J*=5.52 Hz, 1H), 7.81 (dd, *J*=7.25, 8.51 Hz, 1H), 7.77 (t, *J*=7.88 Hz, 1H), 7.60 (d, *J*=7.25 Hz, 1H), 7.56 (d, *J*=7.88 Hz, 1H), 7.40 (s, 1H), 7.21 (d, *J*=7.88 Hz, 1H), 7.25 (br s, 1H), 7.10 (br s, 1H), 5.14 (dd, *J*=5.52, 12.77 Hz, 1H), 3.78 (s, 3H), 3.71 (t, *J*=5.99 Hz, 2H), 3.43-3.61 (m, 10H), 3.36-3.41 (m, 2H), 3.07-3.15 (m, 2H), 2.84-2.95 (m, 1H), 2.68 (t, *J*=5.99 Hz, 2H), 2.52-2.65 (m, 2H), 2.02-2.11 (m, 1H), two protons under DMSO. ^{13}C NMR (125 MHz, DMSO-d_6) δ = 203.4, 173.2, 170.9, 170.3, 168.1, 167.1, 166.4, 165.9, 161.1, 158.3, 157.8, 149.9, 147.9, 136.9, 136.9, 136.6, 131.9, 130.4, 130.0,

128.9, 126.4, 125.5, 120.9, 124.0, 119.5, 118.7, 117.1, 110.2, 101.2, 70.2, 70.2, 70.1, 70.0, 69.5, 66.6, 56.3, 49.4, 39.6, 38.0, 36.8, 31.4, 25.8, 22.4, one carbon not detected. HRMS (*m/z*): $[M+H]^+$ calculated for $C_{44}H_{42}F_3N_7O_{12}$, 917.28435; found, 917.28471. HPLC-MS ^tR = 1.35 min.

(2S,4R)-1-[(2S)-2-(2-{2-[2-(2-azidoethoxy)ethoxy]ethoxy}acetamido)-3,3-dimethyl-butanoyl]-4-hydroxy-N-{[4-(4-methyl-1,3-thiazol-5-yl)phenyl]methyl}pyrrolidine-2-carboxamide (7a). (2*S*,4*R*)-1-[(2*S*)-2-amino-3,3-dimethyl-butanoyl]-4-hydroxy-*N*-[[4-(4-methylthiazol-5-yl)phenyl]methyl]pyrrolidine-2-carboxamide hydrochloride (**2**, 1.000 g, 1 eq) was dissolved in DMF (5 mL). HATU (855 mg, 1.05 eq) and DIPEA (1.28 mL, 3.5 eq) were added. The reaction mixture was stirred for 15 min, then 2-[2-[2-(2-azidoethoxy)ethoxy]ethoxy]acetic acid (524 mg, 1.05 eq) was added. The reaction mixture was stirred at rt for 1 h. The reaction mixture was diluted with EtOAc and washed with a saturated solution of $NaHCO_3$ and then with brine. The organic layer is dried over $MgSO_4$ and evaporated. The residue was purified *via* RP-HPLC under acidic conditions using MeCN/H_2O as eluents in a gradient from 10:90 to 98:2 over 10 min (column: Sunfire™ Prep C18, OBD™ 10 µm, 50x150 mm; flow: 120 mL/min). Product containing fractions were freeze dried to give (2*S*,4*R*)-1-[(2*S*)-2-(2-{2-[2-(2-azidoethoxy)ethoxy]ethoxy}acetamido)-3,3-dimethylbutanoyl]-4-hydroxy-*N*-{[4-(4-methyl-1,3-thiazol-5-yl)phenyl]methyl}pyrrolidine-2-carboxamide (**7a**, 870 mg, 63% yield). ^{1}H NMR (500 MHz, DMSO-d_6) δ = 8.98 (s, 1H), 8.60 (t, *J*=5.99 Hz, 1H), 7.35-7.47 (m, 5H), 4.67-5.61 (m, 1H), 4.57 (d, *J*=9.77 Hz, 1H), 4.32-4.48 (m, 3H), 4.21-4.29 (m, 1H), 3.97 (s, 2H), 3.64-3.69 (m, 1H), 3.53-3.64 (m, 12H), 2.44 (s, 3H), 2.02-2.09 (m, 1H), 1.85-1.94 (m, 1H), 0.93-0.96 (m, 8H), 0.94 (s, 1H), one proton under water. ^{13}C NMR (125 MHz, DMSO-d_6) δ = 172.2, 169.6, 169.1, 152.0, 148.2, 139.9, 131.6, 130.2, 129.2, 127.9, 70.9, 70.4, 70.2, 70.1, 70.1, 69.7,

69.3, 59.2, 57.0, 56.1, 50.4, 42.1, 38.4, 36.2, 26.6, 16.4. HRMS (*m/z*): $[M+H]^+$ calculated for $C_{30}H_{43}N_7O_7S$, 645.29447; found, 645.29442. HPLC-MS ^tR = 1.16 min.

(2S,4R)-1-[(2S)-2-(2-{2-[2-(2-aminoethoxy)ethoxy]ethoxy}acetamido)-3,3-dimethylbutanoyl]-4-hydroxy-N-{[4-(4-methyl-1,3-thiazol-5-yl)phenyl]methyl}pyrrolidine-2-carboxamide (7b). (2*S*,4*R*)-1-[(2*S*)-2-(2-{2-[2-(2-azidoethoxy)ethoxy]ethoxy}acetamido)-3,3-dimethylbutanoyl]-4-hydroxy-*N*-{[4-(4-methyl-1,3-thiazol-5-yl)phenyl]methyl}pyrrolidine-2-carboxamide (**7a**, 1.475 g, 1 eq) was dissolved in MeOH (10 mL), Pd/C (250 mg, 10 %) was added and the mixture was hydrogenated (5 bar H_2 pressure) at rt for 2.5 h. The catalyst was filtered off and the filtrate was purified *via* RP-HPLC under basic conditions using MeCN/H_2O as eluents in a gradient from 10:90 to 90:10 over 10 min. (column: XBridge™ Prep C18, OBD™ 10 µm, 50x150 mm; flow: 140 mL/min). Product containing fractions were freeze dried to give (2*S*,4*R*)-1-[(2*S*)-2-(2-{2-[2-(2-aminoethoxy)ethoxy]ethoxy}acetamido)-3,3-dimethylbutanoyl]-4-hydroxy-*N*-{[4-(4-methyl-1,3-thiazol-5-yl)phenyl]methyl}pyrrolidine-2-carboxamide (**7b**, 1.166 g, 82% yield). ^1H NMR (500 MHz, DMSO-d_6) δ = 9.00 (s, 1H), 8.64 (t, *J*=6.00 Hz, 1H), 7.37-7.49 (m, 5H), 5.17 (br s, 1H), 4.58 (br d, *J*=9.46 Hz, 1H), 4.21-4.48 (m, 4H), 3.99 (s, 2H), 3.65-3.71 (m, 1H), 3.51-3.65 (m, 9H), 3.46 (t, *J*=5.50 Hz, 1H), 2.79 (t, *J*=5.67 Hz, 1H), 2.45 (s, 3H), 2.02-2.11 (m, 1H), 1.86-1.96 (m, 1H), 0.95 (s, 9H), two protons not detected (NH_2). ^{13}C NMR (125 MHz, DMSO-d_6) δ = 172.2, 169.6, 169.1, 152.0, 148.2, 139.9, 131.6, 130.2, 129.2, 127.9, 70.9, 70.4, 70.2, 70.1, 70.1, 70.0, 69.3, 59.2, 57.1, 56.2, 42.1, 38.4, 36.2, 26.7, 16.4, one carbon not detected. HRMS (*m/z*): $[M+H]^+$ calculated for $C_{30}H_{45}N_5O_7S$, 619.30397; found, 619.30333. HPLC-MS ^tR = 1.00 min.

(2S,4R)-4-hydroxy-1-[(2S)-2-(2-{2-[2-(2-{[3-methoxy-4-({4-[(3-oxo-2,3-dihydro-1H-inden-4-yl)oxy]-5-(trifluoromethyl)pyrimidin-2-yl}amino)phenyl]formamido}ethoxy)

ethoxy]ethoxy}acetamido)-3,3-dimethylbutanoyl]-N-{[4-(4-methyl-1,3-thiazol-5-yl)phenyl]methyl}pyrrolidine-2-carboxamide (8, BI-0319). In a 50 mL round-bottom flask, 3-methoxy-4-({4-[(3-oxo-2,3-dihydro-1*H*-inden-4-yl)oxy]-5-(trifluoromethyl)pyrimidin-2-yl}amino)benzoic acid (**2**, 111 mg, 1 eq)was dissolved in DMF (3 mL). DIPEA (96 µl, 3 eq) and HATU (101 mg; 266 µmol; 1.2 eq) were added. The reaction mixture was stirred at rt for 5 min, then (2*S*,4*R*)-1-[(2*S*)-2-[[2-[2-[2-(2-aminoethoxy)ethoxy] ethoxy]acetyl]amino]-3,3-dimethyl-butanoyl]-4-hydroxy-*N*-[[4-(4-methylthiazol-5-yl)phenyl]methyl]pyrrolidine-2-carboxamide (**7b**, 150 mg, 1 eq) was added. The mixture was stirred at rt for 24h. The reaction mixture was diluted with MeCN and H_2O and filtered through a syringe filter prior to purification *via* RP-HPLC under basic conditions using MeCN/H2O as eluents in a gradient from 25:75 to 90:10 over 9 min. (column: XBridge™ Prep C18, OBD™ 10 µm, 50x150 mm; flow: 150 mL/min). The product containing fractions were pooled and freeze-dried to give (2*S*,4*R*)-4-hydroxy-1-[(2*S*)-2-(2-{2-[2-(2-{[3-methoxy-4-({4-[(3-oxo-2,3-dihydro-1*H*-inden-4-yl)oxy]-5-(trifluoromethyl)pyrimidin-2-yl}amino)phenyl]formamido}ethoxy)ethoxy]ethoxy}acetamido)-3,3-dimethylbutanoyl]-*N*-{[4-(4-methyl-1,3-thiazol-5-yl)phenyl]methyl}pyrrolidine-2-carboxamide (**8** (**BI-0319)**, 81 mg, 34% yield) as colorless lyophilizate. ^{1}H NMR (500 MHz, DMSO-d_6) δ = 8.97 (s, 1H), 8.80 (br s, 1H), 8.70 (s, 1H), 8.59 (t, *J*=5.99 Hz, 1H), 8.46 (t, *J*=5.67 Hz, 1H), 7.77 (dd, *J*=7.57, 7.88 Hz, 1H), 7.56 (d, *J*=7.57 Hz, 1H), 7.35-7.46 (m, 6H), 7.21 (d, *J*=7.88 Hz, 1H), 7.23 (br s, 1H), 7.11 (br s, 1H), 5.15 (d, *J*=3.47 Hz, 1H), 4.56 (d, *J*=9.77 Hz, 1H), 4.20-4.48 (m, 4H), 3.96 (s, 2H), 3.77 (s, 3H), 3.36-3.71 (m, 16H), 3.06-3.15 (m, 2H), 2.43 (s, 3H), 2.00-2.10 (m, 1H), 1.85-1.94 (m, 1H), 0.93 (s, 9H). ^{13}C NMR (125 MHz, DMSO-d_6) δ = 203.4, 172.2, 169.6, 169.1, 166.4, 166.0, 161.1, 158.3, 157.8, 151.9, 150.0, 148.2, 147.9, 139.9, 136.9, 131.6, 130.4, 130.2, 130.0, 129.1, 128.9, 127.9, 125.5, 121.0, 124.0, 119.5, 110.2, 101.3,

101.1, 70.9, 70.3, 70.2, 70.1, 70.0, 69.5, 69.3, 59.2, 57.0, 56.3, 56.2, 42.1, 38.4, 36.8, 36.2, 26.6, 25.8, 16.4. HRMS (*m/z*): $[M+H]^+$ calculated for $C_{52}H_{59}F_3N_8O_{11}S$, 1060.39761; found, 1060.39604. HPLC-MS ^tR = 1.35 min.

(2S,4S)-1-[(2S)-2-(2-{2-[2-(2-azidoethoxy)ethoxy]ethoxy}acetamido)-3,3-dimethylbutanoyl]-4-hydroxy-N-{[4-(4-methyl-1,3-thiazol-5-yl)phenyl]methyl}pyrrolidine-2-carboxamide (10a). In a glass vial 2-[2-[2-(2-azidoethoxy) ethoxy] ethoxy]acetic acid (**9**, 569 mg, 1.05 eq) was dissolved in DMF (1 mL) and DIPEA (768 µl, 2 eq). HATU (1.324 g 1.5 eq) and (2*S*,4*S*)-1-[(2*S*)-2-amino-3,3-dimethylbutanoyl]-4-hydroxy-*N*-{[4-(4-methyl-1,3-thiazol-5-yl)phenyl]methyl}pyrrolidine-2-carboxamide (1.000 g, 1 eq) were added. The mixture was stirred at rt for 2 h. The reaction mixture was diluted with EtOAc and washed with a saturated solution of $NaHCO_3$ then with brine. The organic layer was evaporated and the residue was dissolved in MeOH and purified *via* RP-HPLC under acidic conditions using MeCN/H_2O as eluents in a gradient from 15:85 to 98:2 over 10 min (column: Sunfire™ Prep C18, OBD™ 10 µm, 50x150 mm; flow: 120 mL/min). Product containing fractions were freeze dried to give (2*S*,4*S*)-1-[(2*S*)-2-(2-{2-[2-(2-azidoethoxy)ethoxy]ethoxy}acetamido)-3,3-dimethylbutanoyl]-4-hydroxy-*N*-{[4-(4-methyl-1,3-thiazol-5-yl)phenyl]methyl}pyrrolidine-2-carboxamide (**10a**, 700 mg, 47% yield). ^1H NMR (500 MHz, DMSO-d_6) δ = 8.99 (s, 1H), 8.67 (t, *J*=5.99 Hz, 1H), 7.36-7.43 (m, 5H), 5.36 (br s, 1H), 4.52 (d, *J*=9.14 Hz, 1H), 4.18-4.47 (m, 4H), 3.95 (s, 2H), 3.84-3.91 (m, 1H), 3.51-3.64 (m, 11H), 3.43-3.48 (m, 1H), 2.44 (s, 3H), 2.29-2.39 (m, 1H), 1.68-1.79 (m, 1H), 0.96 (s, 9H), one proton under water. ^{13}C NMR (125 MHz, DMSO-d_6) δ = 172.7, 169.8, 169.3, 152.0, 148.2, 139.6, 131.6, 130.2, 129.2, 127.9, 70.9, 70.3, 70.2, 70.1, 70.0, 69.7, 69.5, 59.0, 56.3, 56.1, 50.4, 42.3, 37.4, 35.6, 26.6, 16.4. HRMS (*m/z*): $[M+H]^+$ calculated for $C_{30}H_{43}N_7O_7S$, 645.29447; found, 645.29368. HPLC-MS ^tR = 1.18 min.

(2S,4S)-1-[(2S)-2-(2-{2-[2-(2-aminoethoxy)ethoxy]ethoxy}acetamido)-3,3-dimethyl butanoyl]-4-hydroxy-N-{[4-(4-methyl-1,3-thiazol-5-yl)phenyl]methyl}pyrrolidine-2-carboxamide (10b). In a Parr-reactor (2*S*,4*S*)-1-[(2*S*)-2-(2-{2-[2-(2-azidoethoxy)ethoxy]ethoxy}acetamido)-3,3-dimethylbutanoyl]-4-hydroxy-*N*-{[4-(4-methyl-1,3-thiazol-5-yl)phenyl]methyl}pyrrolidine-2-carboxamide (**10a**, 153 mg, 1 eq) was dissolved in methanol (5 mL) and Pd/C (10%, 25 mg, 0.1 eq) was added. The reactor was flushed with N_2 and filled with H_2 (6 bar). The reaction mixture was allowed to at rt for 3 h. A spoon of celite was added to the reaction mixture, the catalyst was filtered off through a pad of celite and rinsed with DCM and MeOH. The filtrate was concentrated under reduced pressure. (2*S*,4*S*)-1-[(2*S*)-2-(2-{2-[2-(2-aminoethoxy)ethoxy]ethoxy}acetamido)-3,3-dimethylbutanoyl]-4-hydroxy-*N*-{[4-(4-methyl-1,3-thiazol-5-yl)phenyl]methyl}pyrrolidine-2-carboxamide (**10b**, 144 mg, 98% yield) was obtained as colorless resin. The product was taken to the next step without further purification. ^{1}H NMR (500 MHz, DMSO-d_6) δ = 8.99 (s, 1H), 8.72 (br t, *J*=5.83 Hz, 1H), 8.36 (br s, 1H), 7.40 (s, 4H), 5.32 (br s, 1H), 4.52 (d, *J*=9.14 Hz, 1H), 4.18-4.45 (m, 4H), 3.96 (s, 2H), 3.86-3.91 (m, 1H), 3.42-3.62 (m, 11H), 2.82 (br s, 2H), 2.44 (s, 3H), 2.31-2.38 (m, 1H), 1.68-1.79 (m, 1H), 0.96 (s, 9H), two protons not detected (NH_2). ^{13}C NMR (125 MHz, DMSO-d_6) δ = 172.7, 169.8, 169.4, 152.0, 148.2, 139.7, 131.6, 130.2, 129.2, 127.9, 70.8, 70.2, 70.1, 70.1, 70.0, 69.5, 59.0, 56.3, 56.1, 42.3, 37.4, 35.7, 26.6, 16.4, two carbons not detected. HRMS (*m/z*): $[M+H]^+$ calculated for $C_{30}H_{45}N_5O_7S$, 619.30397; found, 619.30308. HPLC-MS ^{t}R = 1.01 min.

(2S,4S)-4-hydroxy-1-[(2S)-2-(2-{2-[2-(2-{[3-methoxy-4-({4-[(3-oxo-2,3-dihydro-1H-inden-4-yl)oxy]-5-(trifluoromethyl)pyrimidin-2-yl}amino)phenyl]formamido}ethoxy) ethoxy]ethoxy}acetamido)-3,3-dimethylbutanoyl]-N-{[4-(4-methyl-1,3-thiazol-5-yl)phenyl]methyl}pyrrolidine-2-carboxamide (11, BI-4206). In a glass vial, 3-methoxy-4-({4-

[(3-oxo-2,3-dihydro-1*H*-inden-4-yl)oxy]-5-(trifluoromethyl)pyrimidin-2-yl}amino)benzoic acid (**2**, 116 mg, 1 eq) was dissolved in DMF (2 mL). DIPEA (100 µL, 3 eq) and HATU (106 mg, 1.2 eq) were added. The reaction mixture was stirred at rt for 5 min, then (2*S*,4*S*)-1-[(2*S*)-2-(2-{2-[2-(2-aminoethoxy)ethoxy]ethoxy}acetamido)-3,3-dimethylbutanoyl]-4-hydroxy-*N*-{[4-(4-methyl-1,3-thiazol-5-yl)phenyl]methyl}pyrrolidine-2-carboxamide (**10b**, 144 mg, 1 eq) was added. The mixture was stirred at rt for 16 h. The reaction mixture was diluted with MeCN and H_2O and filtered through a syringe filter prior to purification *via* RP-HPLC under basic conditions using MeCN/H2O as eluents in a gradient from 30:70 to 98:2 over 8 min (column: YMC Actus-Triart Prep C18, 5 µm, 30x50 mm; flow: 50 mL/min). Product containing fractions were freeze dried to give (2*S*,4*S*)-4-hydroxy-1-[(2*S*)-2-(2-{2-[2-(2-{[3-methoxy-4-({4-[(3-oxo-2,3-dihydro-1*H*-inden-4-yl)oxy]-5-(trifluoromethyl)pyrimidin-2-yl}amino)phenyl]formamido}ethoxy) ethoxy]ethoxy}acetamido)-3,3-dimethylbutanoyl]-*N*-{[4-(4-methyl-1,3-thiazol-5-yl)phenyl]methyl}pyrrolidine-2-carboxamide (**11**, (**BI-4206)**, 169 mg, 69% yield) as off-white lyophilizate. ^{1}H NMR (500 MHz, DMSO-d_6) δ = 8.97 (s, 1H), 8.81 (br s, 1H), 8.70 (s, 1H), 8.66 (t, *J*=5.99 Hz, 1H), 8.45 (t, *J*=5.52 Hz, 1H), 7.77 (dd, *J*=7.57, 7.88 Hz, 1H), 7.56 (d, *J*=7.57 Hz, 1H), 7.35-7.45 (m, 6H), 7.21 (d, *J*=7.88 Hz, 1H), 7.25 (br s, 1H), 7.11 (br s, 1H), 5.45 (br d, *J*=6.62 Hz, 1H), 4.51 (d, *J*=9.14 Hz, 1H), 4.17-4.45 (m, 4H), 3.94 (s, 2H), 3.84-3.91 (m, 1H), 3.77 (s, 3H), 3.36-3.62 (m, 15H), 3.07-3.15 (m, 2H), 2.43 (s, 3H), 2.29-2.36 (m, 1H), 1.69-1.79 (m, 1H), 0.95 (s, 9H). ^{13}C NMR (125 MHz, DMSO-d_6) δ = 203.4, 172.7, 169.8, 169.4, 166.4, 166.0, 161.1, 158.3, 157.8, 151.9, 150.0, 148.2, 147.9, 139.6, 136.9, 131.6, 130.4, 130.2, 130.0, 129.2, 128.9, 127.9, 125.5, 121.0, 124.0, 119.5, 110.2, 101.3, 101.1, 70.9, 70.2, 70.1, 70.1, 70.0, 69.5, 69.5, 59.0, 56.3, 56.1, 42.3, 37.4, 36.8, 35.6, 26.6, 25.8, 16.4, two carbons not detected.

HRMS (*m/z*): $[M+H]^+$ calculated for $C_{52}H_{59}F_3N_8O_{11}S$, 1060.39761; found, 1060.39665. HPLC-MS ^tR = 1.71 min.

Protein expression and purification.

Human PTK2 (residues 411–689, UniProt accession number Q05397) with an N-terminal TEV cleavage site was cloned into pDEST20 vector (Invitrogen). Expression in this vector results in a fusion protein with a cleavable GST tag. Viral stocks were generated in the Bac-to-Bac system (Invitrogen) and used to infect Trichoplusia ni (Hi5) cells (Invitrogen). Recombinant protein was isolated from cell extracts by affinity chromatography over glutathione sepharose (GE Healthcare) in batch mode. The GST-tag was removed by incubation with Ac-TEV protease (ThermoFisher) on the resin, overnight at 4 °C. Cleaved protein was recovered, concentrated (biomax 10, Merck) and finally purified by size exclusion chromatography on HiLoad Superdex S75 (GE Healthcare). The protein was concentrated (biomax 10, Merck) to 5 mg/ml and stored in 20 mM HEPES, 250 mM NaCl, 1 mM DTT, 1 mM EDTA, pH 6.7 at -80 °C.

Crystallization of the PTK2 kinasedomain BI 4464 binary complex.

Protein crystallization was done using the sitting drop method by incubating the protein with 1 mM BI 4464 (as 50 mM stock solution) and mixing 0.2 µL of PTK2 (4.5 mg/mL in 25 mM HEPES pH 6.7, 250 mM NaCl, 1 mM DTT, 1 mM EDTA) with 0.2 µL of reservoir solution (7 % PEG 1500, 100 mM SPG buffer pH 6.0) at 4 °C. Crystals grew as thin plates within a few days to a final size of 150-200 µm). Crystals were transferred to a cryo buffer (reservoir solution with 15 % ethylene glycol) and frozen in liquid nitrogen. Data were collected at the SLS beam line X06DA (Swiss Light Source, Paul Scherrer Institute) at a wavelength of 0.91 Å using the PILATUS 2M detector. The crystals belonged to space group $P2_12_12$ with 1 monomer per asymmetric unit. Images were processed with XDS[48]. The structures were solved by molecular

replacement using the PDB: 2ETM as a search model. Subsequent model building and refinement was done using standard protocols using CCP4[49] , COOT[50] and autoBUSTER[51]. Unit cell parameters were a = 48.05 Å, b = 77.09 Å, c = 82.71 Å and α, β, γ = 90° data and the structure was refined to R and R_{free} values of 18.3 % and 22.2 %, respectively, with 98.1 % of the residues in Ramachandran favored regions as validated with Molprobity[52]. Statistics for data collection and refinement can be found in supplemental table 2. The coordinates and structure factors of the structures have been deposited at the Protein Data Bank with the accession code 6I8Z. The authors will release the atomic coordinates and experimental data upon article publication

Cell culture.

Cell lines were obtained through ATCC or JCRB, verified for identity by satellite repeat analysis, tested for mycoplasm contamination at regular intervals and cultured in the specified media in a humidified cell incubator at 37 °C and 5 % CO_2. DMEM was obtained from Lonza (product code BE12-604F), EMEM from ATCC (product code 30-2003),IMDM from Thermo Fisher (product code 12440053), RPMI-1640 from Thermo Fisher (product code A1049101). The following cell lines (product codes and culture media in parentheses) were used for the described experiments: SNU-387 (CRL-2237, RPMI-1640 plus 10 % heat inactivated FCS), HUH-1 (JCRB0199, DMEM plus 10 % FCS), Hep3B2.1-7 (HB-8064, EMEM plus 10 % FCS), HepG2 (HB-8065, EMEM plus 10 % FCS plus Glutamax), SK-Hep-1 HLF (JCRB0404 DMEM plus 10 % FCS), SNU-398 (CRL-2233, RPMI1640 plus 10 % FCS), HUCCT1 (JCRB0425, RPMI-1640 plus 10 % FCS), HLE (JCRB0405, DMEM plus 10 % FCS), HuH-7 (JCRB0403 DMEM plus 10 % FCS), SNU-423 (CRL-2238, RPMI-1640 plus 10 % FCS), A549 (CCL-185,

F-12K plus 10 % heat inactivated FCS), HSC-3 (JCRB0623, EMEM plus 10 % FCS), C32 (CRL-1585, EMEM plus 10 % FCS), CFPAC-1 (CRL-1918, IMDM plus 10 % FCS).

Protein degradation assays.

To quantify the effects of compounds on PTK2 protein levels, cells were seeded at a density of 125.000 cells in 0.75 mL of culture medium 24-well plates and allowed to attach for 6-8 hours. Subsequently, compounds were added to the cells at logarithmic dose series using the HP Digital Dispenser D300 (Tecan), normalizing for added DMSO. After compound addition, cells were incubated for 18 h or the specified time intervals at 37 °C. Cells were washed with cold PBS and lysed by immediate freezing in 100 µL RIPA buffer (Sigma product code R0278) supplemented with 1:100 HALT Phosphatase-Protease Inhibitors (Thermo product code 1861281) at -80 °C. After thawing, samples were transferred into V-bottom 96-well plates, cellular debris was sedimented at 4000 rpm (Eppendorf centrifuge 5810R, rotor A-4-81). 90 µL of the supernatant were transferred into a new 96-well plate and analyzed using a Wes capillary electrophoresis instrument (Proteinsimple) using PTK2 antibody (Cell Signaling product code 13009) at a dilution of 1:50 or PDE6D antibody (Abcam product code ab5665) at a dilution of 1:25 and GAPDH antibody (Abcam product code ab9485) at a dilution of 1:2000 for normalization.

Proliferation assays.

Standard proliferation assay. To test the effect of PTK2 PROTACs on proliferation, cells were seeded at 1000 cells per well (2500 cells per well for suspension cell lines) in 100 µL growth medium in a white bottom opaque 96-well plate and allowed to grow over night. To obtain starting densities, a set of cells seeded in parallel were lysed and measured using 100 µL CellTiter-Glo luminescent cell viability reagent (Promega product code G7570) per well as per manufacturer's recommendation. Compounds were added to the cells at logarithmic dose series

using the HP Digital Dispenser D300 (Tecan), normalizing for added DMSO. Doxorubicin (Sigma product code D1515) was used as a positive control. Upon compound addition, cells were incubated for six days and viability measured CellTiterGlow reagent as described above. Results are stated as mean and standard deviation of triplicate experiments.

Anchorage independent growth assays. Cells were seeded in 0.3 % agarose (Gibco product code 18300-012) containing cultivation medium (60 µL) on top of a bottom layer composed of 1.2 % agarose in cultivation medium (90 µL) in 96-well plates. Upon solidification of the cell layer, the culture was overlaid with 50 µL cultivation medium and compounds were added as indicated above. Cultures were allowed to grow for 7-14 days, stained with alamar blue reagent (Thermo Fisher product code DAL1025) and measured using a fluorescence plate reader (Wallac Victor 1420, 544 nm excitation, 590 nm emission, 0.2 s).

Long-term proliferation assay. Cells were inoculated at a density of 250,000 cells in 1.5 mL culture medium in 6 well plates. Compounds or DMSO were added, and every 3 to 4 days cells were split to 250,000 cells. Upon splitting, fresh compound was added to keep the concentration constant. Split rates were recorded and multiplied to derive cumulative cell counts which were converted into population doublings (n) using the formula $n = (\log(N_x) - \log(N_0)) / \log 2$ with N_x indicating the cumulative cell count at time-point x and N_0 the initial seeding cell count.

MS proteomics.

Sample preparation. A549 cells were seeded at 5×10^6 cells/mL in a 10 cm plate 18 h before treatment. Cells were treated with 0.1% DMSO as vehicle control, 3 µM of either active PROTAC **6** or **8**, and 3 µM of *cis*VHL **11** as negative control. Cells were incubated at 37 °C and 5 % CO_2 for 18 h before harvesting. Cells were washed twice with DPBS (Gibco) and lysed with

0.5 mL of 100 mM Tris pH 8.0, 4 % (w/v) SDS, supplemented with cOmplete™ Mini EDTA-free Protease Inhibitor Cocktail (Roche). Lysates were sonicated (2 x 10 s) and centrifuged at 14,000 rpm for 20 min at 4 ˚C. The supernatant fraction of the cell extract was collected and protein concentration was quantified by BCA assay (Thermo Fisher Scientific). Further sample processing, digestion, desalting, TMT 10-plex isobaric labelling were performed as previously described.[5] After labelling, the peptides from the 9 samples were pooled together in equal proportion. The pooled sample was fractionated using high pH reverse-phase chromatography on an XBridge peptide BEH column (130 Å, 3.5 μm, 2.1 × 150 mm, Waters) on an Ultimate 3000 HPLC system (Thermo Scientific/Dionex). A mixture of Buffer A (10 mM ammonium formate in water, pH 9) and B (10 mM ammonium formate in 90 % CH3CN, pH 9) was used over a linear gradient of 5 % to 60 % buffer B over 60 min at a flow rate of 200 μL/min. The peptides eluted from the column were collected in 80 fractions before concatenation into 20 fractions based on the UV signal of each fraction. All the fractions were dried in a Genevac EZ-2 concentrator and resuspended in 1 % formic acid for MS analysis.

nLC-MS/MS analysis. The fractions were analyzed sequentially on a Q Exactive HF-X Hybrid Quadrupole-Orbitrap Mass Spectrometer (Thermo Scientific) coupled to an UltiMate 3000 RSLCnano UHPLC system (Thermo Scientific) and EasySpray column (75 μm × 50 cm, PepMap RSLC C18 column, 2 μm, 100 Å, Thermo Scientific). A mix of buffer A (0.1 % formic acid in H_2O) and B (0.08 % formic acid in 80 % CH_3CN) was used over a linear gradient from 5 % to 35 % buffer B over 125 min using a flow rate of 300 nL/min. The column temperature was set at 50 °C. The mass Spectrometer was operated in data dependent mode with a single MS survey scan from 335-1,600 *m/z* followed by 15 sequential *m/z* dependent MS2 scans. The 15 most intense precursor ions were sequentially fragmented by higher energy collision dissociation

(HCD). The MS1 isolation window was set to 0.7 *m/z* and the resolution set at 120,000. MS2 resolution was set at 45,000. The AGC targets for MS1 and MS2 were set at $3e^6$ ions and $1e^5$ ions, respectively. The normalized collision energy was set at 32 %. The maximum ion injection times for MS1 and MS2 were set at 50 ms and 200 ms, respectively.

Peptide and protein identification and quantification. The raw MS data files for all 20 fractions were merged and searched against the Uniprot-sprot-Human-Canonical database by Maxquant software 1.6.0.16 for protein identification and TMT reporter ion quantitation. The identifications were based on the following criteria: enzyme used Trypsin/P; maximum number of missed cleavages equal to two; precursor mass tolerance equal to 10 p.p.m.; fragment mass tolerance equal to 20 p.p.m.; variable modifications: Oxidation (M), Acetyl (N-term), Deamidation (NQ), Gln -> pyro-Glu (Q N-term); fixed modifications: Carbamidomethyl (C). The data was filtered by applying a 1 % false discovery rate followed by exclusion of proteins with less than two unique peptides. Quantified proteins were filtered if the absolute fold-change difference between the three DMSO replicates was ≥ 1.5.

AUTHOR INFORMATION

Corresponding Author

* To whom correspondence should be addressed: Peter Ettmayer, E-mail: peter.ettmayer@boehringer-ingelheim.com

Present Addresses

† Present address (C.M.): Boehringer Ingelheim RCV GmbH & Co KG, 1221, Vienna, Austria.

Author Contributions

The manuscript was written through contributions of all authors. All authors have given approval to the final version of the manuscript.

FUNDING SOURCES

NOTES

While this manuscript was in advanced preparation selective VHL based PTK2 PROTACs were published by P. M. Cromm et al. J. Am. Chem. Soc., DOI: 10.1021/jacs.8b08008 as a manuscript just accepted, describing a VHL-based degrader (PROTAC-3) with chemical structure different from BI-0319.

ACKNOWLEDGMENT

We would like to thank Will Farnaby for coordination of the proteomics study, Moriz Mayer for coordinating the analytics, Gerlinde Flotzinger for PTK2 protein expression and purification, and Gabriele Glenndining and Susanne Mayer for their excellent logistics work for the collaboration between Boehringer Ingelheim and University of Dundee.

ABBREVIATIONS

NH_4OAc, ammonium acetate; BET, bromodomain and extra-terminal; BRD2/3/4/7/9, bromodomain-containing protein 2/3/4/7/9; CRBN, cereblon; DLBCL, Diffuse Large B Cell Lymphoma; HCl, Hydrochloric acid; DIPEA, N,N-Diisopropylethylamine; EtOH, ethanol; EtOAc, ethyl acetate; H_2O, water; HATU, 1-[Bis(dimethylamino)methylene]-1H-1,2,3-triazolo[4,5-b]pyridinium 3-oxid hexafluorophosphate; HOAt, 1-Hydroxy-7-azabenzotriazole

solution; $MgSO_4$, magnesium sulfate; MsCl, methanesolfunyl chloride; PROTAC, proteolysis-targeting chimera; $NaHCO_3$, sodium bicarbonate; NaHDMS, Sodium bis(trimethylsilyl)amide; NaH, sodium hydride; NaOH, sodium hydroxide; $NaIO_4$, sodium periodate; $NaBH(OAc)_3$, sodium triacetoxyborohydride; OsO_4, osmium tetroxide; TEMPO, 2,2,6,6-Tetramethyl-1-piperidinyloxy; VHL; von Hippel-Lindau.

ASSOCIATED CONTENT

Supporting Information

The supporting information is available free of charge on the ACS Publication website at DOI:….

Additional PTK2 degradation data for BI-0319 and BI-3663 in HCC cell lines (SNU387, HUH-1, Hep3B2.1-7, HepG2, SK-Hep1, HLF, SNU-398, HUCCT1, HLE, HuH7, SNU-423); Alamar Blue cell viability assays in above HCC cell lines with BI-3663, BI-0319, BI-4464 and doxorubicine (positive control); Long-term proliferation assays in HSC-3, C32, CFPAC-1 and A549 with 3 μM of of BI-3663 or BI-0319; CRISPR validation of PTK2 dependency, Solubility, plasma protein binding and Caco2 permeability assay data for PROTACs BI-0319 and BI-3663; X-ray Data collection and refinement statistics; Supplementary chemistry information: MS parameters, HPLC chromatograms and NMR spectrum of BI-3663; Supplemental methods: solubility, PPB, CACO2 permeability, stability measurement, CRISPR depletion of PTK2 .

Molecular formula strings (CSV)

Proteomics raw data (XLSX)

Accesion Codes

Atomic coordinates and structure factors for PTK2:BI-4464 have been deposited to the Protein Data Bank (PDB) under accession number 6I8Z. Authors will release the atomic coordinates and experimental data upon article publication

REFERENCES

1. Golubovskaya, V. M. Targeting FAK in human cancer: from finding to first clinical trials. *Front Biosci (Landmark Ed)* **2014,** 19, 687-706.

2. Sulzmaier, F. J.; Jean, C.; Schlaepfer, D. D. FAK in cancer: mechanistic findings and clinical applications. *Nat Rev Cancer* **2014,** 14, 598-610.

3. Lark, A. L.; Livasy, C. A.; Calvo, B.; Caskey, L.; Moore, D. T.; Yang, X.; Cance, W. G. Overexpression of focal adhesion kinase in primary colorectal carcinomas and colorectal liver metastases: immunohistochemistry and real-time PCR analyses. *Clin Cancer Res* **2003,** 9, 215-222.

4. Judson, P. L.; He, X.; Cance, W. G.; Van Le, L. Overexpression of focal adhesion kinase, a protein tyrosine kinase, in ovarian carcinoma. *Cancer* **1999,** 86, 1551-1556.

5. Miyazaki, T.; Kato, H.; Nakajima, M.; Sohda, M.; Fukai, Y.; Masuda, N.; Manda, R.; Fukuchi, M.; Tsukada, K.; Kuwano, H. FAK overexpression is correlated with tumour invasiveness and lymph node metastasis in oesophageal squamous cell carcinoma. *Br J Cancer* **2003,** 89, 140-145.

6. Itoh, S.; Maeda, T.; Shimada, M.; Aishima, S.; Shirabe, K.; Tanaka, S.; Maehara, Y. Role of expression of focal adhesion kinase in progression of hepatocellular carcinoma. *Clin Cancer Res* **2004,** 10, 2812-2817.

7. Sood, A. K.; Armaiz-Pena, G. N.; Halder, J.; Nick, A. M.; Stone, R. L.; Hu, W.; Carroll, A. R.; Spannuth, W. A.; Deavers, M. T.; Allen, J. K.; Han, L. Y.; Kamat, A. A.; Shahzad, M. M.;

McIntyre, B. W.; Diaz-Montero, C. M.; Jennings, N. B.; Lin, Y. G.; Merritt, W. M.; DeGeest, K.; Vivas-Mejia, P. E.; Lopez-Berestein, G.; Schaller, M. D.; Cole, S. W.; Lutgendorf, S. K. Adrenergic modulation of focal adhesion kinase protects human ovarian cancer cells from anoikis. *J Clin Invest* **2010,** 120, 1515-1523.

8. Ward, K. K.; Tancioni, I.; Lawson, C.; Miller, N. L.; Jean, C.; Chen, X. L.; Uryu, S.; Kim, J.; Tarin, D.; Stupack, D. G.; Plaxe, S. C.; Schlaepfer, D. D. Inhibition of focal adhesion kinase (FAK) activity prevents anchorage-independent ovarian carcinoma cell growth and tumor progression. *Clin Exp Metastasis* **2013,** 30, 579-594.

9. Balogh, J.; Victor, D., 3rd; Asham, E. H.; Burroughs, S. G.; Boktour, M.; Saharia, A.; Li, X.; Ghobrial, R. M.; Monsour, H. P., Jr. Hepatocellular carcinoma: a review. *J Hepatocell Carcinoma* **2016,** 3, 41-53.

10. El-Serag, H. B. Hepatocellular carcinoma. *N Engl J Med* **2011,** 365, 1118-1127.

11. Llovet, J. M.; Schwartz, M.; Mazzaferro, V. Resection and liver transplantation for hepatocellular carcinoma. *Semin Liver Dis* **2005,** 25, 181-200.

12. Xu, Q.; Kobayashi, S.; Ye, X.; Meng, X. Comparison of hepatic resection and radiofrequency ablation for small hepatocellular carcinoma: a meta-analysis of 16,103 patients. *Sci Rep* **2014,** 4, 7252.

13. Li, W. X.; Chen, L. P.; Sun, M. Y.; Li, J. T.; Liu, H. Z.; Zhu, W. 3'3-Diindolylmethane inhibits migration, invasion and metastasis of hepatocellular carcinoma by suppressing FAK signaling. *Oncotarget* **2015,** 6, 23776-23792.

14. Gnani, D.; Romito, I.; Artuso, S.; Chierici, M.; De Stefanis, C.; Panera, N.; Crudele, A.; Ceccarelli, S.; Carcarino, E.; D'Oria, V.; Porru, M.; Giorda, E.; Ferrari, K.; Miele, L.; Villa, E.; Balsano, C.; Pasini, D.; Furlanello, C.; Locatelli, F.; Nobili, V.; Rota, R.; Leonetti, C.; Alisi, A.

Focal adhesion kinase depletion reduces human hepatocellular carcinoma growth by repressing enhancer of zeste homolog 2. *Cell Death Differ* **2017,** 24, 889-902.

15. Hirt, U. A.; Waizenegger, I. C.; Schweifer, N.; Haslinger, C.; Gerlach, D.; Braunger, J.; Weyer-Czernilofsky, U.; Stadtmuller, H.; Sapountzis, I.; Bader, G.; Zoephel, A.; Bister, B.; Baum, A.; Quant, J.; Kraut, N.; Garin-Chesa, P.; Adolf, G. R. Efficacy of the highly selective focal adhesion kinase inhibitor BI 853520 in adenocarcinoma xenograft models is linked to a mesenchymal tumor phenotype. *Oncogenesis* **2018,** 7, 21.

16. Tiede, S.; Meyer-Schaller, N.; Kalathur, R. K. R.; Ivanek, R.; Fagiani, E.; Schmassmann, P.; Stillhard, P.; Hafliger, S.; Kraut, N.; Schweifer, N.; Waizenegger, I. C.; Bill, R.; Christofori, G. The FAK inhibitor BI 853520 exerts anti-tumor effects in breast cancer. *Oncogenesis* **2018,** 7, 73.

17. Tanjoni, I.; Walsh, C.; Uryu, S.; Tomar, A.; Nam, J. O.; Mielgo, A.; Lim, S. T.; Liang, C.; Koenig, M.; Sun, C.; Patel, N.; Kwok, C.; McMahon, G.; Stupack, D. G.; Schlaepfer, D. D. PND-1186 FAK inhibitor selectively promotes tumor cell apoptosis in three-dimensional environments. *Cancer Biol Ther* **2010,** 9, 764-777.

18. Cance, W. G.; Golubovskaya, V. M. Focal adhesion kinase versus p53: apoptosis or survival? *Sci Signal* **2008,** 1, pe22.

19. Sakamoto, K. M.; Kim, K. B.; Kumagai, A.; Mercurio, F.; Crews, C. M.; Deshaies, R. J. Protacs: chimeric molecules that target proteins to the Skp1-Cullin-F box complex for ubiquitination and degradation. *Proc Natl Acad Sci U S A* **2001,** 98, 8554-8559.

20. Ottis, P.; Crews, C. M. Proteolysis-targeting chimeras: induced protein degradation as a therapeutic strategy. *ACS Chem Biol* **2017,** 12, 892-898.

21. Collins, I.; Wang, H.; Caldwell, J. J.; Chopra, R. Chemical approaches to targeted protein degradation through modulation of the ubiquitin-proteasome pathway. *Biochem J* **2017,** 474, 1127-1147.

22. Lai, A. C.; Crews, C. M. Induced protein degradation: an emerging drug discovery paradigm. *Nat Rev Drug Discov* **2017,** 16, 101-114.

23. Hughes, S. J.; Ciulli, A. Molecular recognition of ternary complexes: a new dimension in the structure-guided design of chemical degraders. *Essays Biochem* **2017,** 61, 505-516.

24. Nowak, R. P.; DeAngelo, S. L.; Buckley, D.; He, Z.; Donovan, K. A.; An, J.; Safaee, N.; Jedrychowski, M. P.; Ponthier, C. M.; Ishoey, M.; Zhang, T.; Mancias, J. D.; Gray, N. S.; Bradner, J. E.; Fischer, E. S. Plasticity in binding confers selectivity in ligand-induced protein degradation. *Nat Chem Biol* **2018**, 706-714.

25. Gadd, M. S.; Testa, A.; Lucas, X.; Chan, K. H.; Chen, W.; Lamont, D. J.; Zengerle, M.; Ciulli, A. Structural basis of PROTAC cooperative recognition for selective protein degradation. *Nat Chem Biol* **2017,** 13, 514-521.

26. Chan, K. H.; Zengerle, M.; Testa, A.; Ciulli, A. Impact of target warhead and linkage vector on inducing protein degradation: comparison of bromodomain and extra-terminal (BET) degraders derived from triazolodiazepine (JQ1) and tetrahydroquinoline (I-BET726) BET inhibitor scaffolds. *J Med Chem* **2018,** 61, 504-513.

27. Bondeson, D. P.; Smith, B. E.; Burslem, G. M.; Buhimschi, A. D.; Hines, J.; Jaime-Figueroa, S.; Wang, J.; Hamman, B. D.; Ishchenko, A.; Crews, C. M. Lessons in PROTAC design from selective degradation with a promiscuous warhead. *Cell Chem Biol* **2018,** 25, 78-87 e5.

28. Zengerle, M.; Chan, K. H.; Ciulli, A. Selective small molecule induced degradation of the BET bromodomain protein BRD4. *ACS Chem Biol* **2015,** 10, 1770-1777.

29. Remillard, D.; Buckley, D. L.; Paulk, J.; Brien, G. L.; Sonnett, M.; Seo, H. S.; Dastjerdi, S.; Wuhr, M.; Dhe-Paganon, S.; Armstrong, S. A.; Bradner, J. E. Degradation of the BAF complex factor BRD9 by heterobifunctional ligands. *Angew Chem Int Ed Engl* **2017,** 56, 5738-5743.

30. Winter, G. E.; Buckley, D. L.; Paulk, J.; Roberts, J. M.; Souza, A.; Dhe-Paganon, S.; Bradner, J. E. Drug development: phthalimide conjugation as a strategy for in vivo target protein degradation. *Science* **2015,** 348, 1376-1381.

31. Lai, A. C.; Toure, M.; Hellerschmied, D.; Salami, J.; Jaime-Figueroa, S.; Ko, E.; Hines, J.; Crews, C. M. Modular PROTAC design for the degradation of oncogenic BCR-ABL. *Angew Chem Int Ed Engl* **2016,** 55, 807-810.

32. Petroski, M. D.; Deshaies, R. J. Function and regulation of cullin-RING ubiquitin ligases. *Nat Rev Mol Cell Biol* **2005,** 6, 9-20.

33. Zhu, Y. X.; Braggio, E.; Shi, C. X.; Bruins, L. A.; Schmidt, J. E.; Van Wier, S.; Chang, X. B.; Bjorklund, C. C.; Fonseca, R.; Bergsagel, P. L.; Orlowski, R. Z.; Stewart, A. K. Cereblon expression is required for the antimyeloma activity of lenalidomide and pomalidomide. *Blood* **2011,** 118, 4771-4779.

34. Powell, C. E.; Gao, Y.; Tan, L.; Donovan, K. A.; Nowak, R. P.; Loehr, A.; Bahcall, M.; Fischer, E. S.; Janne, P. A.; George, R. E.; Gray, N. S. Chemically induced degradation of anaplastic lymphoma kinase (ALK). *J Med Chem* **2018,** 61, 4249-4255.

35. Huang, H. T.; Dobrovolsky, D.; Paulk, J.; Yang, G.; Weisberg, E. L.; Doctor, Z. M.; Buckley, D. L.; Cho, J. H.; Ko, E.; Jang, J.; Shi, K.; Choi, H. G.; Griffin, J. D.; Li, Y.; Treon, S.

P.; Fischer, E. S.; Bradner, J. E.; Tan, L.; Gray, N. S. A chemoproteomic approach to query the degradable kinome using a multi-kinase degrader. *Cell Chem Biol* **2018,** 25, 88-99 e6.

36. McDonald, E. R., 3rd; de Weck, A.; Schlabach, M. R.; Billy, E.; Mavrakis, K. J.; Hoffman, G. R.; Belur, D.; Castelletti, D.; Frias, E.; Gampa, K.; Golji, J.; Kao, I.; Li, L.; Megel, P.; Perkins, T. A.; Ramadan, N.; Ruddy, D. A.; Silver, S. J.; Sovath, S.; Stump, M.; Weber, O.; Widmer, R.; Yu, J.; Yu, K.; Yue, Y.; Abramowski, D.; Ackley, E.; Barrett, R.; Berger, J.; Bernard, J. L.; Billig, R.; Brachmann, S. M.; Buxton, F.; Caothien, R.; Caushi, J. X.; Chung, F. S.; Cortes-Cros, M.; deBeaumont, R. S.; Delaunay, C.; Desplat, A.; Duong, W.; Dwoske, D. A.; Eldridge, R. S.; Farsidjani, A.; Feng, F.; Feng, J.; Flemming, D.; Forrester, W.; Galli, G. G.; Gao, Z.; Gauter, F.; Gibaja, V.; Haas, K.; Hattenberger, M.; Hood, T.; Hurov, K. E.; Jagani, Z.; Jenal, M.; Johnson, J. A.; Jones, M. D.; Kapoor, A.; Korn, J.; Liu, J.; Liu, Q.; Liu, S.; Liu, Y.; Loo, A. T.; Macchi, K. J.; Martin, T.; McAllister, G.; Meyer, A.; Molle, S.; Pagliarini, R. A.; Phadke, T.; Repko, B.; Schouwey, T.; Shanahan, F.; Shen, Q.; Stamm, C.; Stephan, C.; Stucke, V. M.; Tiedt, R.; Varadarajan, M.; Venkatesan, K.; Vitari, A. C.; Wallroth, M.; Weiler, J.; Zhang, J.; Mickanin, C.; Myer, V. E.; Porter, J. A.; Lai, A.; Bitter, H.; Lees, E.; Keen, N.; Kauffmann, A.; Stegmeier, F.; Hofmann, F.; Schmelzle, T.; Sellers, W. R. Project DRIVE: a compendium of cancer dependencies and synthetic lethal relationships uncovered by large-scale, deep RNAi screening. *Cell* **2017,** 170, 577-592 e10.

37. Galdeano, C.; Gadd, M. S.; Soares, P.; Scaffidi, S.; Van Molle, I.; Birced, I.; Hewitt, S.; Dias, D. M.; Ciulli, A. Structure-guided design and optimization of small molecules targeting the protein-protein interaction between the von Hippel-Lindau (VHL) E3 ubiquitin ligase and the hypoxia inducible factor (HIF) alpha subunit with in vitro nanomolar affinities. *J Med Chem* **2014,** 57, 8657-8663.

38. Fischer, E. S.; Bohm, K.; Lydeard, J. R.; Yang, H.; Stadler, M. B.; Cavadini, S.; Nagel, J.; Serluca, F.; Acker, V.; Lingaraju, G. M.; Tichkule, R. B.; Schebesta, M.; Forrester, W. C.; Schirle, M.; Hassiepen, U.; Ottl, J.; Hild, M.; Beckwith, R. E.; Harper, J. W.; Jenkins, J. L.; Thoma, N. H. Structure of the DDB1-CRBN E3 ubiquitin ligase in complex with thalidomide. *Nature* **2014,** 512, 49-53.

39. Bondeson, D. P.; Mares, A.; Smith, I. E.; Ko, E.; Campos, S.; Miah, A. H.; Mulholland, K. E.; Routly, N.; Buckley, D. L.; Gustafson, J. L.; Zinn, N.; Grandi, P.; Shimamura, S.; Bergamini, G.; Faelth-Savitski, M.; Bantscheff, M.; Cox, C.; Gordon, D. A.; Willard, R. R.; Flanagan, J. J.; Casillas, L. N.; Votta, B. J.; den Besten, W.; Famm, K.; Kruidenier, L.; Carter, P. S.; Harling, J. D.; Churcher, I.; Crews, C. M. Catalytic in vivo protein knockdown by small-molecule PROTACs. *Nat Chem Biol* **2015,** 11, 611-617.

40. Lu, J.; Qian, Y.; Altieri, M.; Dong, H.; Wang, J.; Raina, K.; Hines, J.; Winkler, J. D.; Crew, A. P.; Coleman, K.; Crews, C. M. Hijacking the E3 ubiquitin ligase cereblon to efficiently target BRD4. *Chem Biol* **2015,** 22, 755-763.

41. Soares, P.; Gadd, M. S.; Frost, J.; Galdeano, C.; Ellis, L.; Epemolu, O.; Rocha, S.; Read, K. D.; Ciulli, A. Group-based optimization of potent and cell-active inhibitors of the von Hippel-Lindau (VHL) E3 ubiquitin ligase: structure-activity relationships leading to the chemical probe (2S,4R)-1-((S)-2-(1-cyanocyclopropanecarboxamido)-3,3-dimethylbutanoyl)-4-hydroxy -N-(4-(4-methylthiazol-5-yl)benzyl)pyrrolidine-2-carboxamide (VH298). *J Med Chem* **2018,** 61, 599-618.

42. Frost, J.; Galdeano, C.; Soares, P.; Gadd, M. S.; Grzes, K. M.; Ellis, L.; Epemolu, O.; Shimamura, S.; Bantscheff, M.; Grandi, P.; Read, K. D.; Cantrell, D. A.; Rocha, S.; Ciulli, A.

Potent and selective chemical probe of hypoxic signalling downstream of HIF-alpha hydroxylation via VHL inhibition. *Nat Commun* **2016,** 7, 13312.

43. Soucy, T. A.; Smith, P. G.; Milhollen, M. A.; Berger, A. J.; Gavin, J. M.; Adhikari, S.; Brownell, J. E.; Burke, K. E.; Cardin, D. P.; Critchley, S.; Cullis, C. A.; Doucette, A.; Garnsey, J. J.; Gaulin, J. L.; Gershman, R. E.; Lublinsky, A. R.; McDonald, A.; Mizutani, H.; Narayanan, U.; Olhava, E. J.; Peluso, S.; Rezaei, M.; Sintchak, M. D.; Talreja, T.; Thomas, M. P.; Traore, T.; Vyskocil, S.; Weatherhead, G. S.; Yu, J.; Zhang, J.; Dick, L. R.; Claiborne, C. F.; Rolfe, M.; Bolen, J. B.; Langston, S. P. An inhibitor of NEDD8-activating enzyme as a new approach to treat cancer. *Nature* **2009,** 458, 732-736.

44. Saeki, T.; Ueda, K.; Tanigawara, Y.; Hori, R.; Komano, T. Human P-glycoprotein transports cyclosporin A and FK506. *J Biol Chem* **1993,** 268, 6077-6080.

45. Chessum, N. E. A.; Sharp, S. Y.; Caldwell, J. J.; Pasqua, A. E.; Wilding, B.; Colombano, G.; Collins, I.; Ozer, B.; Richards, M.; Rowlands, M.; Stubbs, M.; Burke, R.; McAndrew, P. C.; Clarke, P. A.; Workman, P.; Cheeseman, M. D.; Jones, K. Demonstrating In-cell target engagement using a pirin protein degradation probe (CCT367766). *J Med Chem* **2018,** 61, 918-933.

46. Meyers, R. M.; Bryan, J. G.; McFarland, J. M.; Weir, B. A.; Sizemore, A. E.; Xu, H.; Dharia, N. V.; Montgomery, P. G.; Cowley, G. S.; Pantel, S.; Goodale, A.; Lee, Y.; Ali, L. D.; Jiang, G.; Lubonja, R.; Harrington, W. F.; Strickland, M.; Wu, T.; Hawes, D. C.; Zhivich, V. A.; Wyatt, M. R.; Kalani, Z.; Chang, J. J.; Okamoto, M.; Stegmaier, K.; Golub, T. R.; Boehm, J. S.; Vazquez, F.; Root, D. E.; Hahn, W. C.; Tsherniak, A. Computational correction of copy number effect improves specificity of CRISPR-Cas9 essentiality screens in cancer cells. *Nat Genet* **2017,** 49, 1779-1784.

47. Stadtmueller, H.; Sapountzis, I. Preparation of Pyrimidinamine Derivatives for Treating Diseases Characterized by Excessive or Abnormal Cell Proliferation. *Int Pat Appl* WO 2010/058032, May 27, **2010**.

48. Kabsch, W. Integration, scaling, space-group assignment and post-refinement. *Acta Crystallogr D Biol Crystallogr* **2010,** 66, 133-144.

49. Dodson, E. J.; Winn, M.; Ralph, A. Collaborative computational project, number 4: providing programs for protein crystallography. *Methods Enzymol* **1997,** 277, 620-633.

50. Emsley, P.; Lohkamp, B.; Scott, W. G.; Cowtan, K. Features and development of Coot. *Acta Crystallogr D Biol Crystallogr* **2010,** 66, 486-501.

51. Bricogne, G.; Blanc, E.; Brandl, M.; Flensburg, C.; Keller, P.; Paciorek, W.; Roversi, P.; Sharff, A.; Smart, O. S.; Vonrhein, C.; Womack, T. O. *BUSTER version 2.11.5*. Global Phasing Ltd: Cambridge, United Kingdom, 2011.

52. Chen, V. B.; Arendall, W. B., 3rd; Headd, J. J.; Keedy, D. A.; Immormino, R. M.; Kapral, G. J.; Murray, L. W.; Richardson, J. S.; Richardson, D. C. MolProbity: all-atom structure validation for macromolecular crystallography. *Acta Crystallogr D Biol Crystallogr* **2010,** 66, 12-21.

Table of Contents graphic

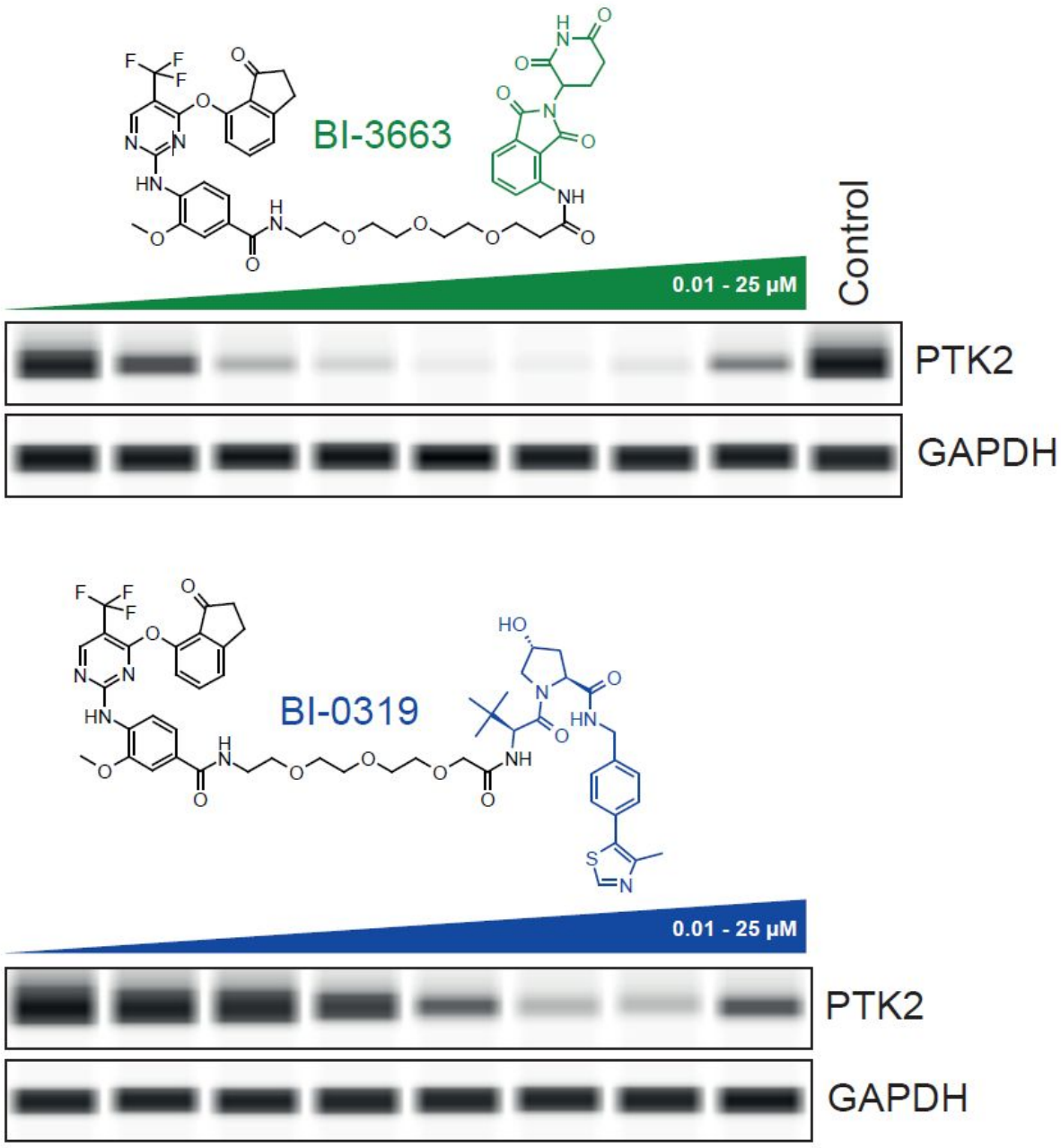

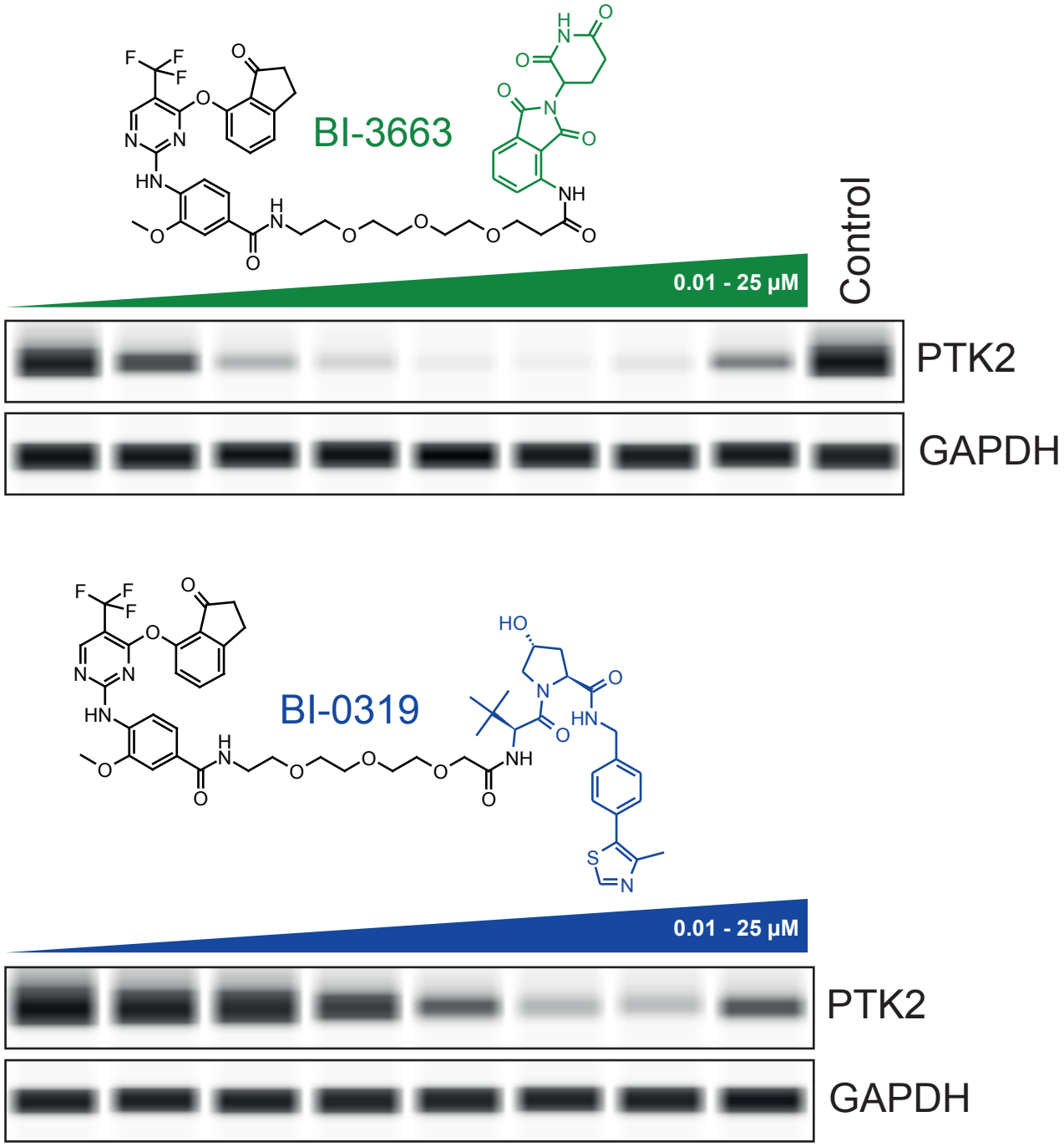
BI-3663
0.01 - 25 µM
Control
PTK2
GAPDH
BI-0319
0.01 - 25 µM
PTK2
GAPDH